Developmental Testbed Center (DTC) Project for the Air Force

Final report documenting:
GSI mitigation support (1.5.4)
GSI data sensitivity tests (1.5.1)

February 2015

Index

1. Introduction

The Gridpoint Statistical Interpolation (GSI) Data Assimilation (DA) System is a three dimensional (3D-Var) variational and hybrid DA system currently used by various agencies as part of operational systems for both regional and global applications, including NCEP's Global Forecast System (GFS), North American Mesoscale Forecast System (NAM), and Hurricane WRF (HWRF) Forecast System, NASA's Global Forecast System as well as NOAA's Rapid Refresh (RAP) and High Resolution RAP (HRRR). The GSI is also a community research model with public access. The DTC provides code management and central user support to the user community as well as facilitates code

transitions from research to operations. The DTC annually releases an updated GSI code to the research community, along with an updated users' guide and an on-site user tutorial.

Since 2009, the DTC has been performing baseline experiments designed to assist the Air Force in determining an appropriate configuration for the Air Force regional DA system. For FY2014, DTC tests were particularly focused on sensitivity studies of traditional and non-traditional data types as identified by the Air Force. Through these sensitivity tests, the DTC is tasked with providing recommendations to the Air Force on how best to configure the GSI DA system to optimize the utility of these data. Additionally, the DTC was tasked to provide mitigation support for GSI operations. For all sensitivity tests and mitigation experiments, the DTC runs a functionally-similar testing environment aimed to complement the real-time pre-operational Air Force system.

This report is split into two separate sections corresponding to the two sub-tasks in the statement of work (SOW):

- Mitigation of GSI Issues (Task 1.5.4)
- Sensitivity tests on traditional and non-traditional observation sources (Task 1.5.1)

Section 2 covers the mitigation task. In-depth analysis on the source of Sea Level Pressure analysis errors are discussed in sub-section a, which begins where the FY2013 final report concluded with discussion of post-processor discrepancies and focuses on the GSI and the Advanced and Research Weather and Forecasting model (ARW) balance. Sub-section b gives a short overview of a mitigation request from the Air Force to address Cross-track Infrared Sounder (CrIS) data usage in the operational system. Section 3 covers the data sensitivity studies. Sub-sections a-c describes the background, experiment design, and impact of raising the model top from 10 hPa to 2 hPa, respectively. Sub-section d focuses on the ozone data types, Solar Backscatter Ultraviolet (SBUV/2; sub-section i) and Global Ozone Monitoring Experiment (GOME-2; sub-section ii), followed by CrIS data impacts in sub-section e. Finally, results from the forecast sensitivity to observations (FSO) system are described in sub-section f followed by conclusions in sub-section g. Section 4 is the appendix, which includes the GSI and ARW namelists.

2. Mitigation of GSI Issues

a. Sea level pressure analysis errors

The Air Force discovered problems in the sea level pressure (SLP) field when implementing GSI on their southwest Asia (T4) domain. Figure 2.a.1 is a time series of bias and root-mean-square error (RMSE) of SLP provided by the Air Force in July, 2013. A large RMSE was shown, particularly in the analysis time for the SLP field derived from GSI, relative to the RMSE for the current (in July 2013) operational production system (WRFDA). Similar behavior was reported by the Air Force for all other verification time periods.

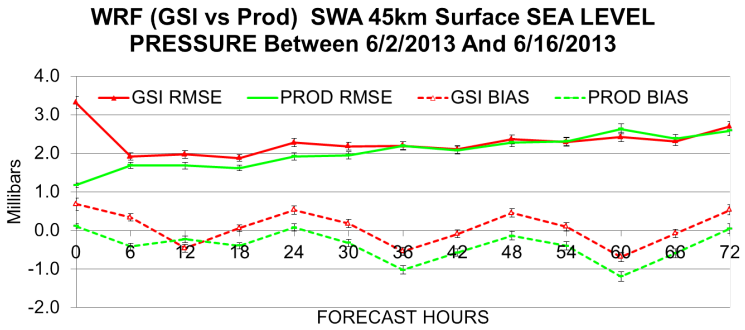

Figure 2.a.1: Surface Sea Level Pressure for SW Asia domain for two week forecast period in June, 2013. Red lines indicate GSI RMSE (solid) and Bias (dashed) and green lines indicate WRFDA RMSE (solid) and Bias (dashed).

Figure 2.a.2 shows SLP fields for both the background (6 hour forecast from previous 06 UTC cycle) and analysis using GSI for 20131114 at 12 UTC. Areas of high SLP bias in the analysis are circled in yellow. The circled areas are not present in the background, as well as the WRFDA analysis (not shown). This indicates an issue specific to the calculation of SLP and/or associated components of the testing system including GSI.

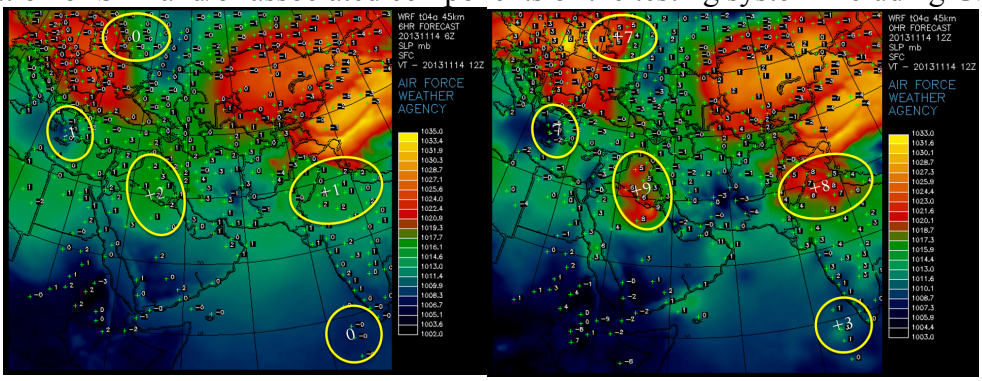

Figure 2.a.2: SLP fields for the background (left) and generated from the GSI experiment (right). SLP values are contoured, with fit to observations (Analysis-observation) values overlaid. Yellow circles indicate areas of high bias.

i. Post-processing discrepancies

Quality control issues for surface temperature and moisture inside GSI was identified and code changes were proposed and tested in FY2013. Although these changes did show some marked improvement (not shown), the anomalously large SLP biases in the GSI analysis still persisted. It should be noted that SLP is not an analysis variable, nor a forecast variable, therefore it is not directly updated by the data assimilation system (either GSI or WRFDA here), or the forecast model, ARW. Because of this, the FY2013 project report suggested a closer look at the post-processor methods and calculations used to determine SLP. A consistent challenge for the DTC was the inability to reproduce the post-processed SLP values produced by the Air Force for the same case. Figure 2.a-i.1 shows the difference in post-processed SLP fields for the same analysis between the Air Force and the DTC, which is characterized by areas of considerably higher SLP values in

the Air Force product relative to the DTC. The DTC uses the Unified Post Processor (UPP), whereas the Air Force uses a version of the WRF Post Processor (WPP).

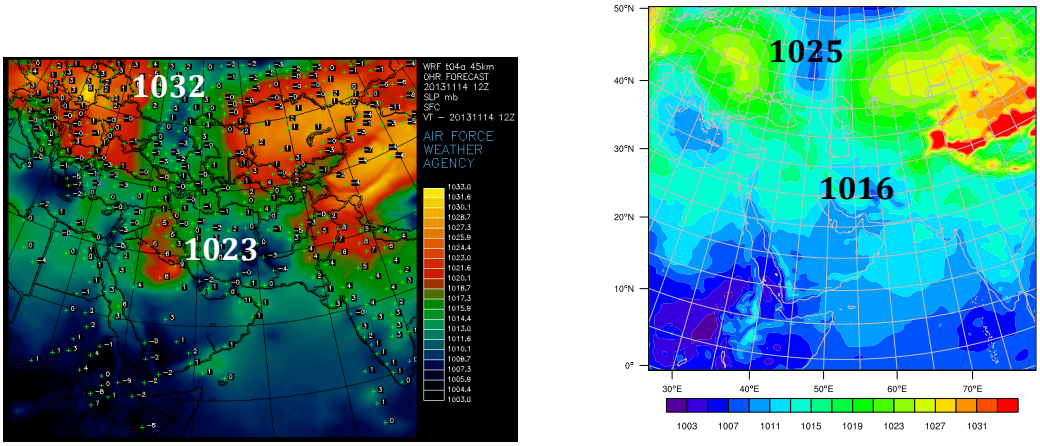

Figure 2.a-i.1: Post-processor discrepancies between the Air Force SLP (left; WPP) and the DTC SLP (right; UPP).

The Air Force delivered their post-processing routines to calculate the SLP to the DTC, and the differences were examined. The major differences in the routines were the source of pressure used to compute the SLP: the Air Force routine uses perturbation pressure at the lowest model level, whereas UPP uses dry air mass in column (MU) and water vapor (UPP for RAP applications uses surface pressure). It was found that there were two keys to reproducing the high biases in the SLP field:

- The input file for WPP/UPP must be the ARW output file at the analysis time (i.e. 0-hour forecast file generated by ARW, not wrfinput directly generated from GSI analysis)
- Perturbation pressure at the lowest model level (P'(0,:,:)) needs to be used for surface pressure in the SLP computation, not MU or the surface pressure (Psfc) directly from GSI

These points raised the question of what the differences are between the GSI analysis (wrfinput) and the ARW analysis (wrfout; 0-hr forecast) files, and further, why does the WRFDA analysis file not produce the erroneously high SLP values in the postprocessor? Figure 2.a-i.2 shows the differences between the ARW analysis file (wrfout at 0 hour) and the GSI analysis (wrfinput) and between the ARW analysis file (wrfout at 0 hour) and the WRFDA analysis (wrfinput) for the 1st level P' field. When comparing the two DA systems, it is clear the GSI P' field has some inconsistencies with the ARW P' field, whereas the WRFDA analysis file has a consistent P' field with ARW. It is important to point out the GSI does not update P', therefore the difference in Figure 2.a-i2 shows the difference between the ARW analysis and the GSI background files. However, such a discrepancy suggests that the output from GSI is different from what ARW expects.

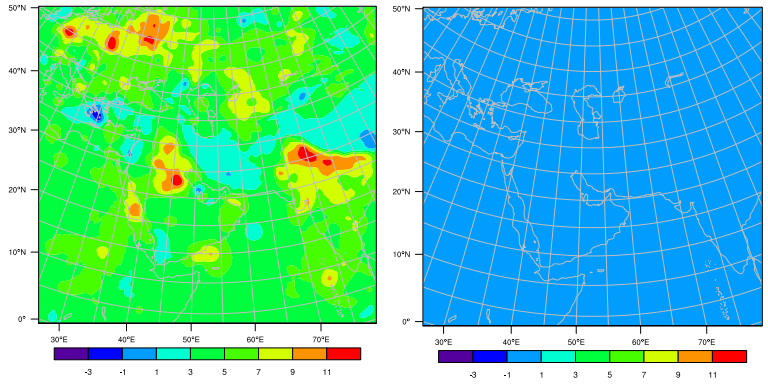

Figure 2.a-i.2: 1st level perturbation pressure + base state pressure for the ARW 0-hr forecast – GSI analysis (left) and ARW 0-hr forecast – WRFDA analysis (right).

ii. Increment tests (WRFDA vs. GSI)

In order to take a closer look at the resulting P' differences between the ARW analysis and the GSI background (0-hr forecast – background), the components in the ARW analysis calculation were diagnosed. The diagnostic relation for the full pressure (vapor plus dry air) is as follows:

$$p = p_0(R_d\theta_m/p_0\alpha_d)^\gamma$$

Eqn. 2.a.ii-1

where $\theta_m = \theta(1 + (R_v/R_d)q_v) \approx \theta(1 + 1.61q_v)$, q_v is the mixing ratio for water vapor and α_d is the inverse density of dry air. These variables are among the analysis control variables the ARW expects from the data assimilation system, GSI or WRFDA here, to compute the diagnostic variables. In order to isolate the impact of each control variable, all other analysis increments were turned off in GSI (only the increment of interest was applied to the background) to test the contribution to P' in the ARW calculation. Figure 2.a-ii.1 shows that the temperature and moisture increments predominately make up the resulting P' field, whereas the MU field has much less impact of the result of P'.

P' increment
All

P' increment
T(0,:,:) only

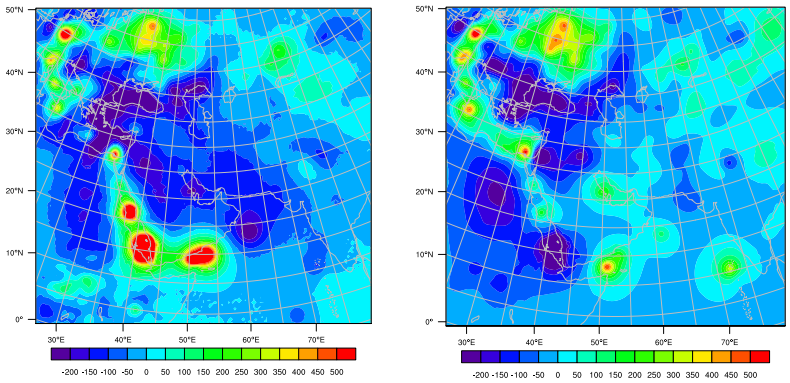

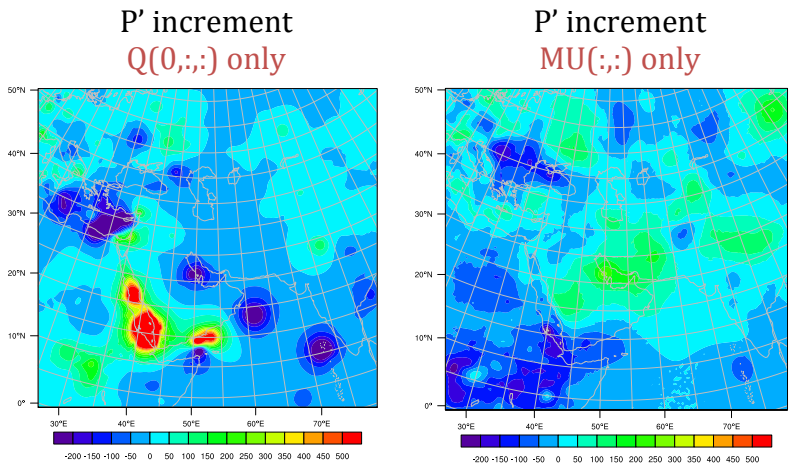

Figure 2.a-ii.1: P' increment in ARW 0-hr forecast with all variables turned on (top left), with only T increments in GSI (top right), only QVAPOR increments in GSI (bottom left), and only MU increments in GSI (bottom right).

Furthermore, the differences between the analysis control variables in GSI and WRFDA are shown in Figures 2.a-ii.2 – 2.a.ii.4 for specific humidity (QVAPOR), Temperature (T), and MU, respectively. Generally, WRFDA and GSI show similar magnitude of QVAPOR increments, except the large increment around 10°N from GSI (Figure 2.a-ii.2). The anomaly increment may be due to a bad surface moisture observation that was not filtered out by the quality control (QC). Updates to the surface QC were proposed in FY2013, however these updates have not been applied to these tests as a precaution to resolve the underlying problem before implementing the suggested increased QC. Figure 2.a-ii.3 shows a large difference in the temperature increment fields with the WRFDA field producing a more "smooth" and spatially expansive field. This indicates that the WRFDA system is likely adding an extra adjustment to the temperature field rather than simply adding the analysis increment to the background. The MU field is shown in Figure 2.a-ii.4, which is characterized by larger magnitude and larger spatial coverage in the WRFDA increment relative to the GSI increment.

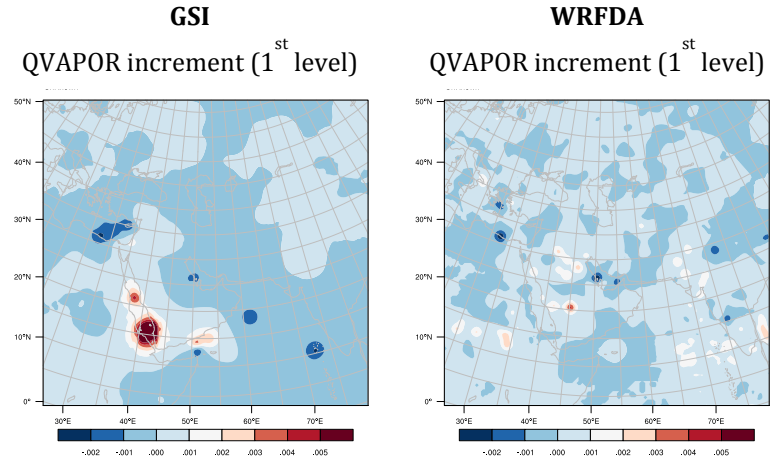

Figure 2.a-ii.2: 1st level QVAPOR increment for GSI (left) and WRFDA (right) DA systems.

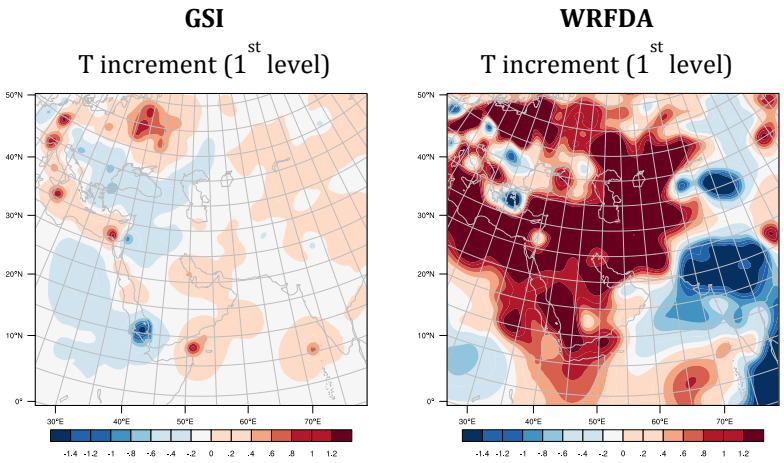

Figure 2.a-ii.3: 1st level temperature increment for GSI (left) and WRFDA (right) DA systems.

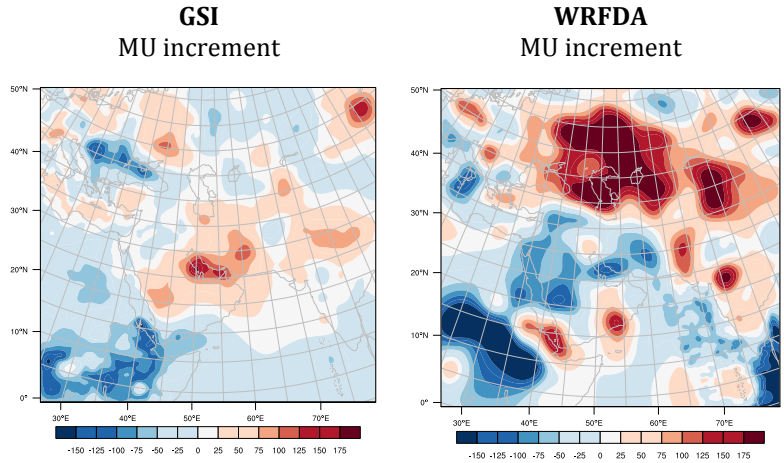

Figure 2.a-ii.4: 1st level MU increment for GSI (left) and WRFDA (right) DA systems.

iii. WRFDA, ARW, and RAP rebalance formulation

After performing update to the analysis variables, WRFDA includes a subroutine, `da_transfer_xatowrf`, to derive increments for diagnostic variables $\Delta\theta, \Delta P, \Delta\phi, \Delta\mu$ based on analysis increments, $\Delta T, \Delta P_s, \Delta q$. WRFDA computes:

Increments of mixing ratio water vapor (q) at level k:

$$q'_k = \frac{qv'_k}{\left(1 - qv_k\right)^2} \qquad \text{Eqn 2.a-iii.1}$$

Increments of MU (μ):

$$\underline{\mu'} = \frac{p'_{sfc} - (\mu + \mu') \times \int_0^{1.0} q'_k \, d\eta w}{1 + \int_0^{1.0} q_k \, d\eta w} = - \frac{p'_{sfc} + (\mu + \mu') \times \int_{1.0}^{0} q'_k \, d\eta w}{\int_{1.0}^{0} (1 + q_k) d\eta w} \qquad \text{Eqn 2.a-iii.2}$$

Increments of the pressure (p) at level k obtained from increments of surface pressure and water vapor mixing ratio:

$$p'_{\eta w\_k} = p'_{\eta w\_k+1} + \int_{\eta w\_k}^{\eta w+k+1} \left\{ \underline{\mu'} \times (1+q_k) + (\overline{\mu} + \mu') \times q'_k \right\} d\eta w \quad k = kte, \ldots, kts. \qquad \text{Eqn 2.a-iii.3}$$

$$p'_{\eta w\_kte+1} = 0.0 \qquad p'_k = \frac{p'_{\eta w+k+1} + p'_{\eta w+k}}{2}$$

where ,
Increments of potential temperature (θ) at level k:

$$\theta_k = t_k \times \left(\frac{p_k}{p_{00}} \right)^{-\frac{R}{c_p}} \qquad \text{Eqn 2.a-iii.5a}$$

$$\theta'_k = \theta_k \times \left(\frac{t'_k}{t_k} - \frac{R}{c_p} \frac{p'_k}{p_k} \right) \qquad \text{Eqn 2.a-iii.5b}$$

Increments of geopotential height (φ) at level $k+1$:

$$\varphi'_{k+1} = \varphi'_k - \int_{\eta w\_k}^{\eta w\_k+1} \left(\frac{\mu'}{\rho_k} + (\mu + \mu') \times \frac{\rho'_k}{\rho_k^2} \right) d\eta w, \quad k = kts, \ldots, kte. \qquad \text{Eqn 2.a-iii.6}$$

Unlike WRFDA, GSI does not have such a subroutine to perform additional increment calculations. GSI uses $\Delta T, \Delta P_s, \Delta q, \Delta \mu$ and computes θ from background T, P_s.

When ARW initializes, prognostic variables are re-computed based on the input file, wrfinput, either from the WRF Preprocessing System (WPS)-*real* or the data assimilation system. As a result, wrfout file is generated at the analysis time and the variables contained in this file are used inside ARW as the initial conditions for forecasts. The prognostic variables in ARW are as follows:

$$\partial_t U + (\nabla \cdot \mathbf{V} u) + \mu_d \alpha \partial_x p + (\alpha/\alpha_d) \partial_\eta p \partial_x \phi = F_U \qquad \text{Eqn 2.a-iii.7a}$$

$$\partial_t V + (\nabla \cdot \mathbf{V} v) + \mu_d \alpha \partial_y p + (\alpha/\alpha_d) \partial_\eta p \partial_y \phi = F_V \qquad \text{Eqn 2.a-iii.7b}$$

$$\partial_t W + (\nabla \cdot \mathbf{V} w) - g[(\alpha/\alpha_d) \partial_\eta p - \mu_d] = F_W \qquad \text{Eqn 2.a-iii.7c}$$

$$\partial_t \Theta + (\nabla \cdot \mathbf{V} \theta) = F_\Theta \qquad \text{Eqn 2.a-iii.7d}$$

$$\partial_t \mu_d + (\nabla \cdot \mathbf{V}) = 0 \qquad \text{Eqn 2.a-iii.7e}$$

$$\partial_t \phi + \mu_d^{-1} [(\mathbf{V} \cdot \nabla \phi) - gW] = 0 \qquad \text{Eqn 2.a-iii.7f}$$

$$\partial_t Q_m + (\nabla \cdot \mathbf{V} q_m) = F_{Q_m} \qquad \text{Eqn 2.a-iii.7g}$$

where F_U, F_V, and F_W are momentum (U, V, and W are wind components, respectively), followed by the equations for mass: F_Θ (temperature), μ_d (dry air), and ϕ (geopotential), and finally F_{Qm} (water vapor). The diagnostic equations for dry inverse density and full pressure (vapor plus dry air) are as follows:

$$\partial_\eta \phi = -\alpha_d \mu_d \qquad \text{Eqn 2.a-iii.8a}$$

$$p = p_0 (R_d \theta_m / p_0 \alpha_d)^\gamma \qquad \text{Eqn 2.a-iii.8b}$$

These diagnostic equations are used by WPS-*real.* Therefore when the input file (wrfinput) comes from *real*, the content of the input file and the WRF re-computed analysis file are consistent. When a DA system is added into the workflow (wrfinput is instead coming from the analysis), the diagnostic variables are recomputed based on either the analysis variables or the background for those that are not updated by the data assimilation system (GSI or WRFDA here). Besides the pressure fields mentioned earlier, another discrepancy between the prognostic variables for ARW and the GSI analysis control variables is geopotential height (ϕ). ϕ is a prognostic variable in ARW, whereas GSI does not update its values. However, WRFDA computes a geopotential height increment through the subroutine `da_transfer_xatowrf`, as mentioned earlier (Eqn 2.a-iii.5).

iv. RAP case

The Rapid Refresh (RAP) operational system at NOAA GSD is most similar to the Air Force operational system in that the GSI is coupled with the ARW dynamical core. Therefore, DTC staff consulted with NOAA/GSD colleagues working with the RAP to investigate whether similar problems existed in the RAP system, and how these inconsistencies at the initial time are handled for the RAP system. Figure 2.a-iv.1 show the RAP partial cycle on 2014061515 for P' difference between the GSI analysis and the 0-hr ARW forecast before and after the digital filter initialization (DFI) step and the subsequent rebalance. Figure 2.a-iv.2 shows the same figure for the RAP full cycle on 2014061515. Both the partial and full cycles show that the RAP system has considerable P' differences without the DFI and rebalance steps, and elimination of these differences after the DFI and rebalance. The RAP team has considerable interest in this issue as the HRRR uses the same system, however DFI is not a good option for the HRRR given the convective scale for which it resolves. Currently the HRRR is initialized by the RAP, but once it is migrated to full cycling, the same initialization issues in the P' field as the Air Force has seen in their operational system will be present. Work to include a rebalance step was undertaken at GSD. The DTC has followed this work and tested it for Air Force applications.

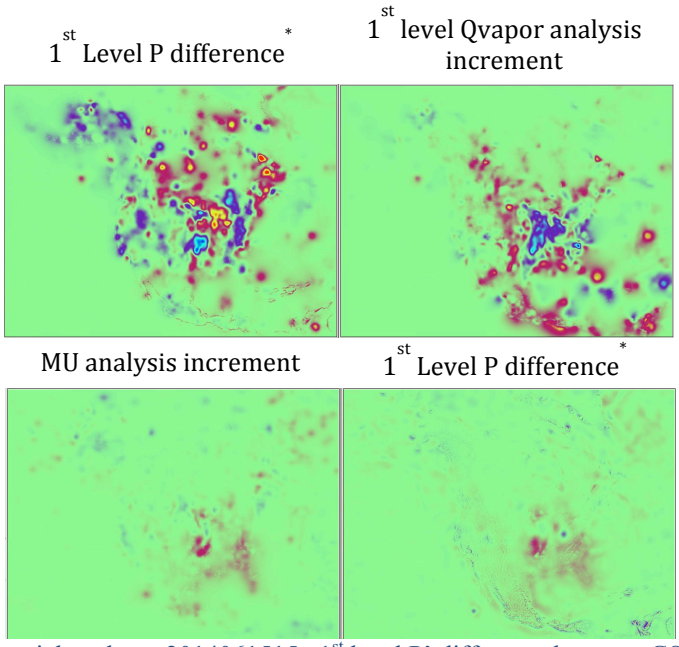

Figure 2.a-iv.1: RAP partial cycle on 2014061515. 1st level P' difference between GSI analysis and 0-hr ARW forecast without DFI and rebalance (top left), 1st level QVAPOR increment (top right), MU analysis increment (bottom left), and 1st level P' difference between GSI and 0-hr ARW forecast after DFI and rebalance (bottom right).

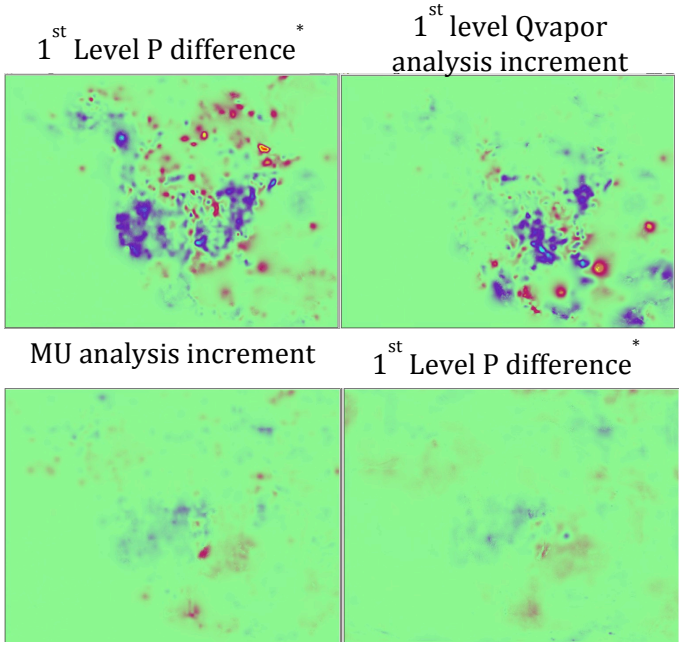

Figure 2.a-iv.2: Same as 2.a-iv.1 expect for full cycle.

v. Rebalance tests

Equations 2.a-v.1 – 2.a-v4 show the rebalance calculation used by RAP. They are applied to perturbation pressure, specific volume and geopotential height, which are calculated using T, μ, and q.

Perturbation pressure at level *kte*:

$$p'_{kte} = -\frac{1}{2}\int_{\eta w_{kte}}^{\eta w_{kte+1}} \left(\mu' + q'_{kte} \times \left(\mu' + \overline{\mu}\right)\right) d\eta w = -\frac{1}{2}\int_{\eta w_{kte}}^{\eta w_{kte+1}} \frac{\left(\mu' + \frac{q'_{kte}}{1+q'_{kte}} \times \overline{\mu}\right)}{\left(\frac{1}{1+q'_{kte}}\right)} \times \frac{1}{\left(\frac{1}{d\eta w}\right)}$$ Eqn 2.a-v.1

Perturbation pressure at level *k* between levels *kte-1* to *kts*:

$$p'_k = p'_{k+1} - \int_{\eta_k}^{\eta_{k+1}} \left(\mu' + \frac{\left(q'_{k+1} + q'_k\right)}{2} \times \left(\mu' + \overline{\mu}\right)\right) d\eta = p'_{k+1} - \int_{\eta_k}^{\eta_{k+1}} \frac{\left(\mu' + \frac{0.5 \times \left(q'_{k+1} + q'_k\right)}{1+0.5 \times \left(q'_{k+1} + q'_k\right)} \times \overline{\mu}\right)}{\left(\frac{1}{1+0.5 \times \left(q'_{k+1} + q'_k\right)}\right)} \times \frac{1}{\left(\frac{1}{d\eta}\right)}$$ Eqn 2.a-v.2

Perturbation of the specific volume at level *k* :

$$\alpha'_k = \frac{R}{p_{00}} \times \left(\theta'_k + \theta_0\right) \times \left(1 + \frac{R_v}{R_d} q'_k\right) \times \left(\frac{p'_k + \overline{p}_k}{p_{00}}\right)^{-\frac{c_v}{c_p}} - \overline{\alpha}_k$$ Eqn 2.a-v.3

Perturbation of the geopotential height at level *k*:

$$\varphi'_k = \varphi'_{k-1} - \int_{\eta w_{k-1}}^{\eta w_k} \left(\left(\mu' + \overline{\mu}\right) \times \alpha'_{k-1} + \mu' \times \overline{\alpha}_{k-1} \right) d\eta w$$ Eqn 2.a-v.4

1) *Analysis test*

In order to see the noise that is present in the initial time steps, Figure 2.a-1.1 shows the change in surface pressure with time for each WRF time step for a single cycle (2014080106), with the first 5 time steps highlighted. The GSI run without rebalance shows a large dPs/dt in the initial 3-4 time steps before leveling off, whereas the GSI run with the rebalance shows a stable dPs/dt.

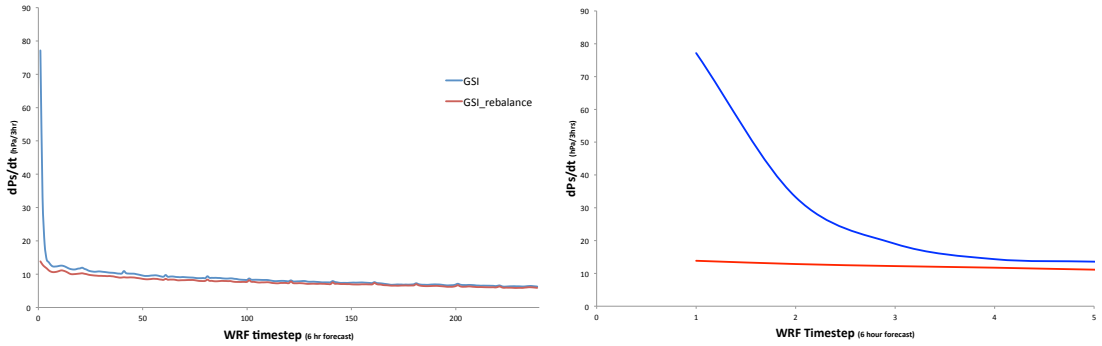

Figure 2.a-1.1: Change in surface pressure with time (dPs/dt) for the GSI without rebalance (blue) and GSI without rebalance in the ARW (red). Full 6 hr forecast cycle (left) with zoomed in view of the first 5 time steps (right).

The difference in the perturbation pressure field between the GSI analysis and the ARW 0-hr forecast is an indication of how much the diagnostic computation of P is changing between GSI and ARW (indication of the balance). Figure 2.a-1.2 shows the GSI P' difference field before and after the rebalance is applied, as well as the rebalance with the geopotential height update removed. The resulting P' difference field after the rebalance is applied vastly reduces the differences from the GSI run without rebalance, with the P' difference after rebalance being very close to the background field. The test without the update to geopotential shows the amount that the geopotential height variable contributes to this solution.

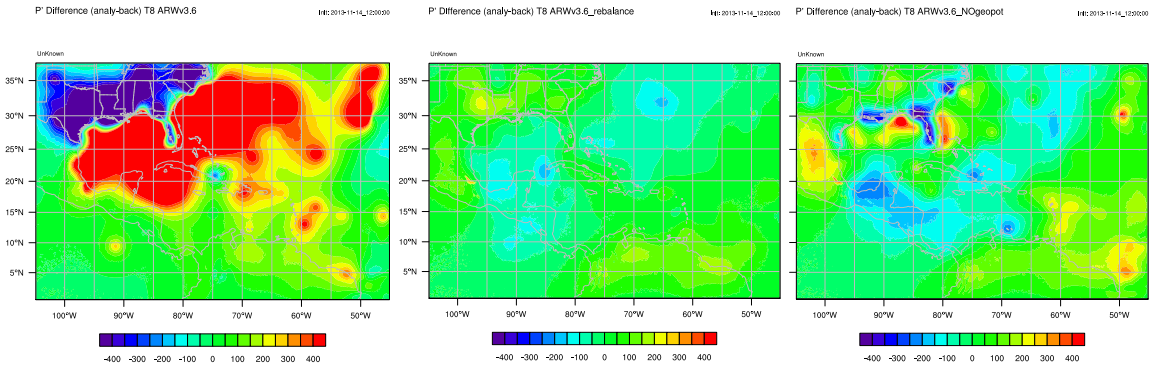

Figure 2.a-1.2: Perturbation pressure difference between the GSI analysis and the ARW 0-hr forecast for the GSI without rebalance (left), GSI with rebalance (center), and GSI with rebalance but without update to the geopotential variable (right).

Although the problem stems from the difference in P' when ARW initializes from a GSI analysis without an incremented geopotential height variable, the Mean SLP (MSLP) field was the initial problem reported by the Air Force and therefore may be of interest. Therefore, Figure 2.a-1.3 shows the resulting MSLP field (using UPP modified to use 1st level perturbation pressure rather than MU or surface pressure for the calculation) with and without rebalance. The results show a smoother MSLP field with less erroneously high MSLP values.

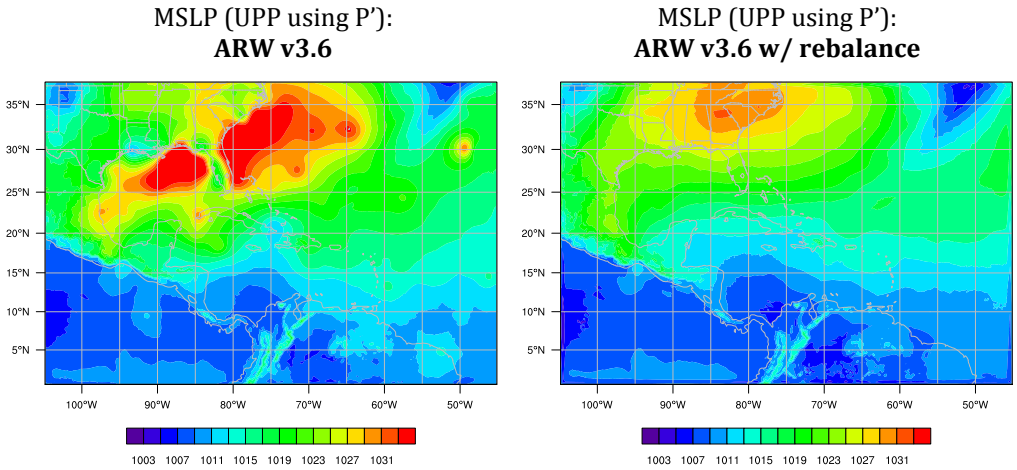

Figure 2.a-1.3: Mean SLP field calculated using 1st level P' for the surface pressure without (left) and with (right) rebalance applied.

2) *Forecast results*

The unbalanced state in the P' field when running GSI with ARW only appears to affect the analysis time and first few forecast hours before the forecast system establishes a balanced state. Therefore, the affect of the rebalance on the forecast is an important consideration. Figures 2.a-2.1 – 2.a-2.4 show the 12-hour, 24-hour, and 48-hour forecast for geopotential height, zonal wind, specific humidity, and temperature, respectively for a 10-day test using the Air Force operational configuration. The GSI with rebalance tends to statistically significantly (SS; 95%) outperform the GSI without rebalance at 1-3 vertical levels at the 12-hour forecast time for each of the variables, with a single (two) SS degradation in the GSI with rebalance (relative to the GSI without rebalance) in the geopotential height (temperature) fields. However, by 24-hours, those improvements are primarily gone or replaced with SS differences favoring the GSI without rebalance. Most notable are the SS degradations with using the rebalance in the mid-level temperature forecasts. When comparing the GSI with rebalance to a run without DA, most of the differences are not SS between the two runs. This suggests that using the current rebalance algorithm wipes out most of the improvements for the DA and pushes the analysis too close to the background.

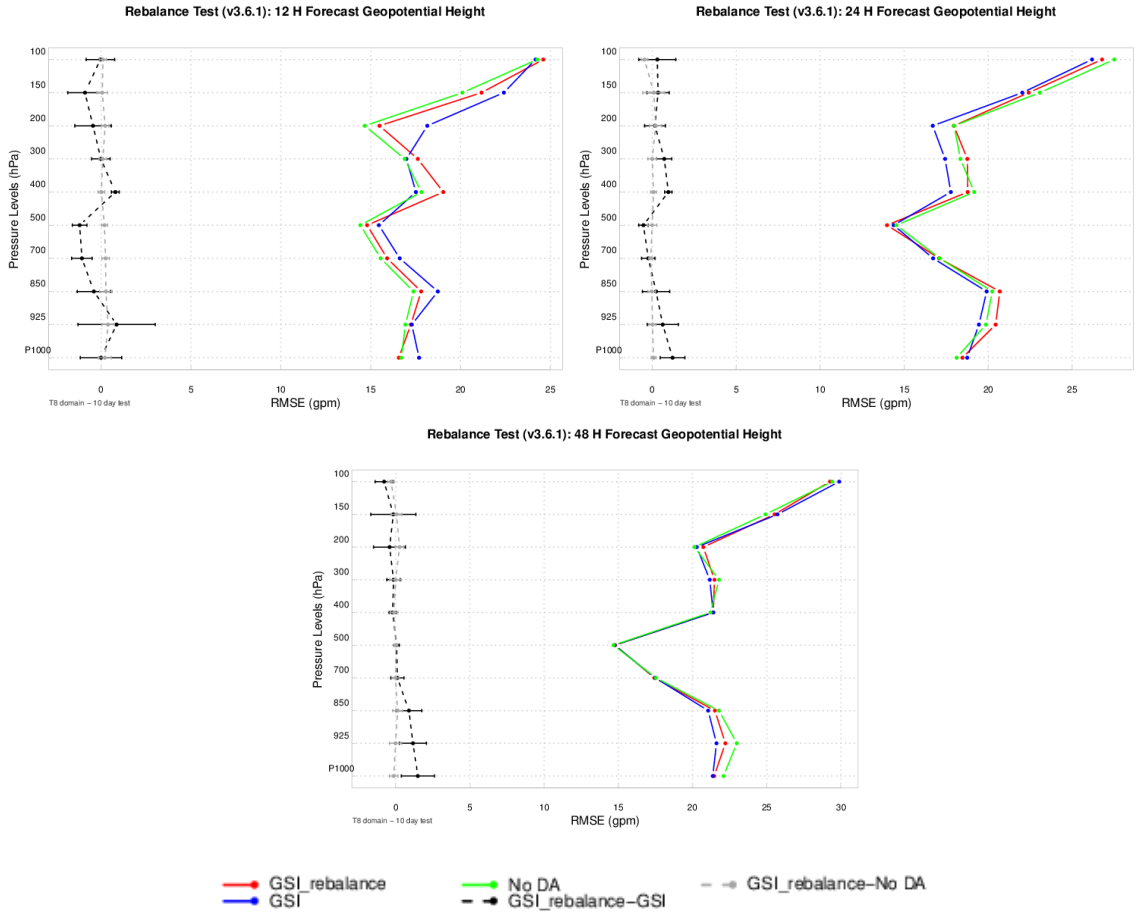

Figure 2.a-2.1: Rebalance test forecasts for geopotential height at 12-hour (top left), 24-hour (top right), and 48-hour (lower) forecasts. The GSI with rebalance (red) is compared to the GSI without rebalance (blue) with the pairwise difference of these two runs in black. The no-data assimilation run (green) and GSI with rebalance pairwise difference is in grey. Differences are not SS when the confidence interval (CI) does not encompass zero.

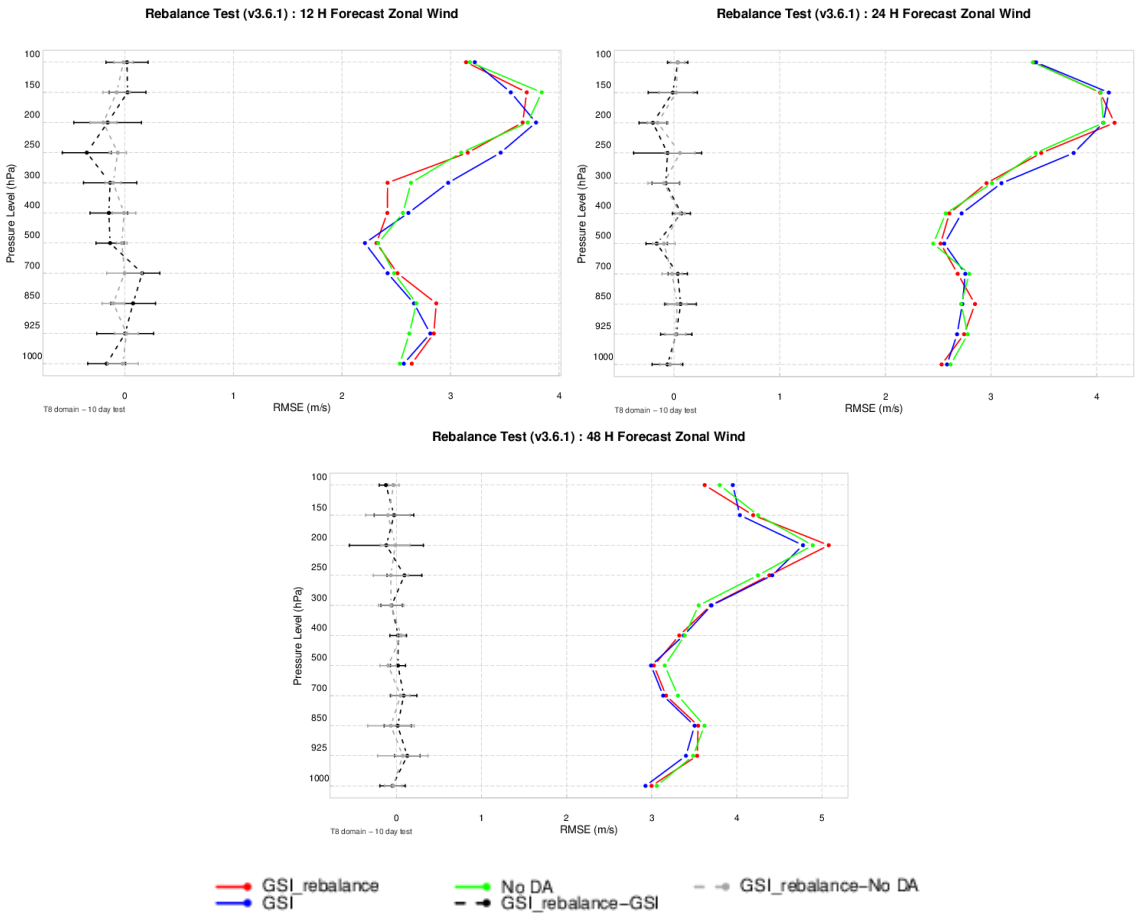

Figure 2.a-2.2: Same as 2.a-2.1 except zonal wind.

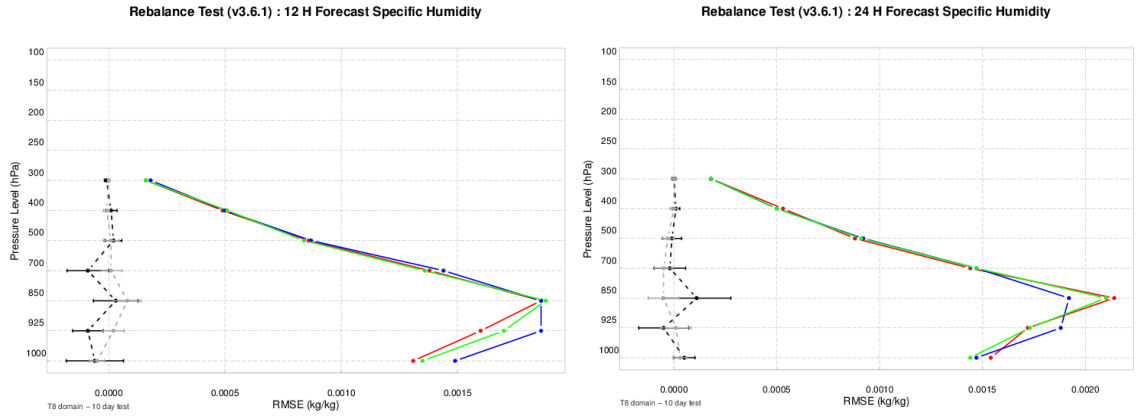

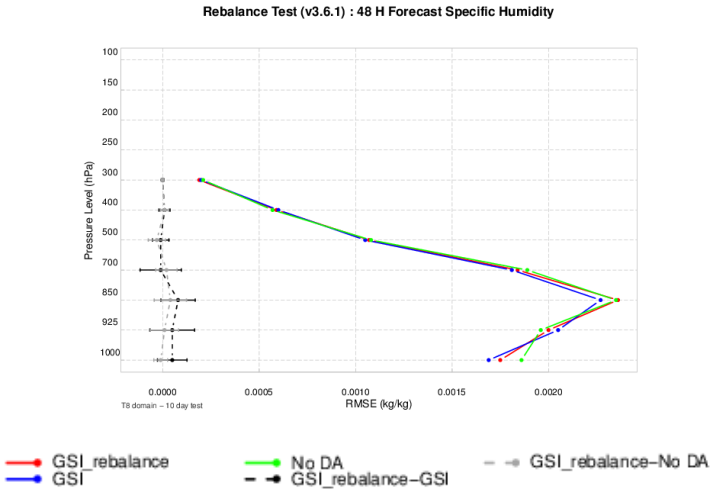

Figure 2.a-2.3: Same as 2.a-2.1 except specific humidity.

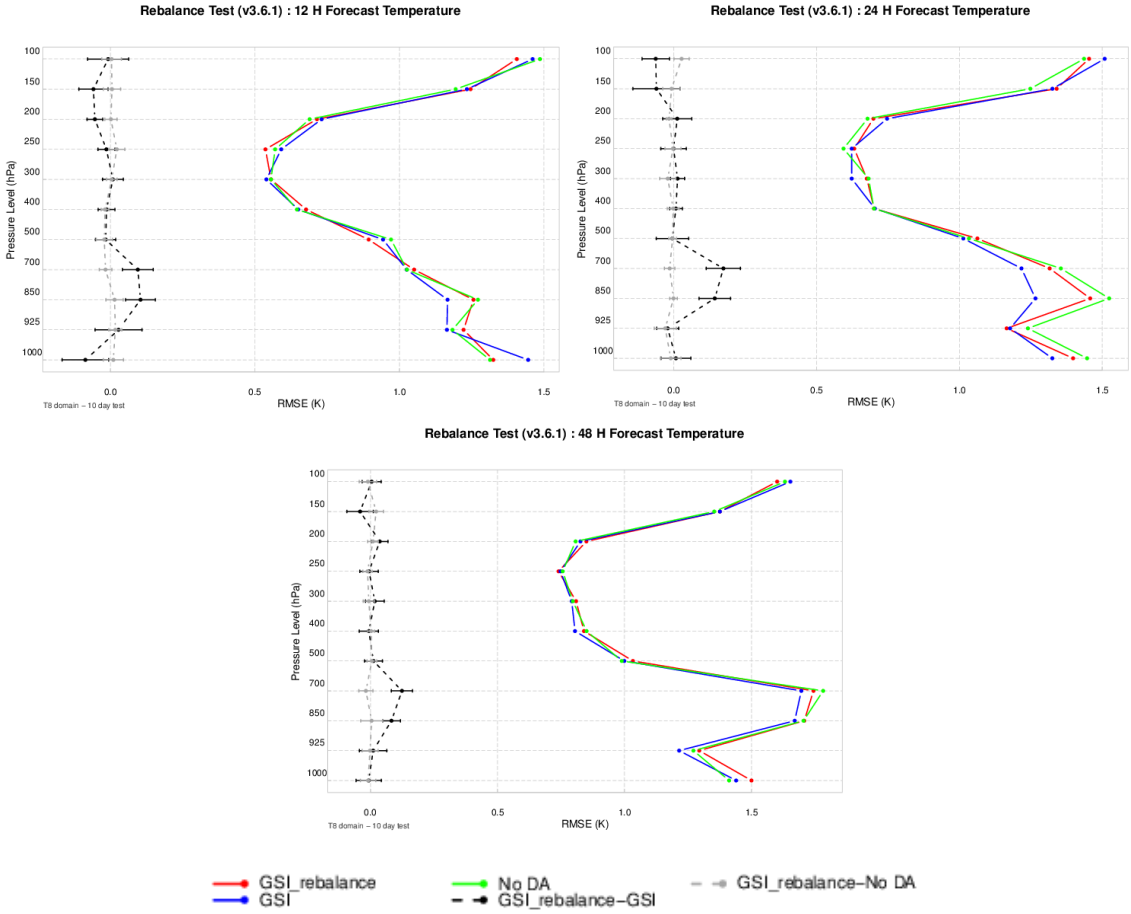

Figure 2.a-2.4: same as 2.a-2.1 except temperature

vi. Conclusions

The reason for the large SLP errors in the Air Force operational analysis when using GSI was traced back to a mismatch in the GSI analysis and the ARW 0-hr forecast. This difference stems from the difference between the prognostic variables used by ARW and analysis variables used by GSI. This is not a rare problem when the forecast model and its data assimilation system were developed independently. Table 2.a-vi.1 shows a summary of the control and prognostic variables for the DA and forecast systems, respectively as well as the computed or diagnostic variables for each system.

Table 2.a-vi.1: Summary of differences in WRFDA, GSI, Rebalance, and ARW formulas

	WRFDA	GSI	Rebalance	ARW
Control/prognostic variables	$\Delta T\ \Delta P_s\ \Delta q$	$\Delta T\ \Delta P_s\ \Delta q\ \Delta \mu$	$T\ \mu\ q$	$\phi\ \mu\ \theta$
Computed/diagnostic variables	$\Delta\theta\ \Delta P\ \Delta\phi\ \Delta\mu$	$\Delta\theta$ *(from* ΔT*)*	$P\ \alpha\ \phi$	$\alpha\ P$

The important distinction between the WRFDA formulation and the RAP rebalance algorithm is that the WRFDA uses increment fields, whereas the RAP rebalance uses full fields. The current direction of the HRRR developers is to implement the rebalance approach. Forecast tests show that applying the rebalance algorithm to the GSI analysis (right before running ARW) benefits initial 6- and 12-hour forecasts, but degrading the longer (24- to 48-hour) forecasts. For those longer forecasts, the rebalance run shows non-SS differences relative to the no data assimilation run, indicating the rebalance may be pushing too close back to the background and removing many of the DA benefits at longer lead times.

Future work discussions suggest that investigating the addition of an appropriate rebalance algorithm posterior to GSI when interfacing with ARW may be a promising direction. Further studies should be performed on how to perform such a rebalance (e.gl, applied to increment fields or full fields) and which fields should be applied to. Furthermore, surface observation internal QC (FY2013 work) should be implemented to remove bad surface observations from being ingested into GSI.

b. CrIS data usage

The Air Force submitted a mitigation request pertaining to a significant decrease in the CrIS data assimilated when using GSI v3.2 (with Forecast Sensitivity to Observations; FSO) rather than GSI v3.1 (Air Force operational configuration at time of request). DTC requested a case and was able to reproduce the decrease in number of observations assimilated, shown in Table 2.b.1.

Table 2.b.1: DTC comparison to Air Force case for CrIS mitigation request

			# Read	# Kept	# Assimilated
GSI v3.1	**T4 DTC repeat**				
	npp	cris	1695750	468825	12797
	T4 Air Force				
	npp	cris	551019	156009	15954
GSI v3.2	**FSO DTC repeat**				
	npp	cris	1231713	318402	1074
	FSO Air Force				
	npp	cris	1231713	318402	1074

The problem was identified in the use of the GSI namelist option 'dval'. In GSI v3.1 dval=1 and in GSI v3.2 dval=0 for CrIS (other types dval=1 for v3.2). When dval =0, this leads to most of the CrIS data being tossed by the radiance thinning process. This option allows for relative weighting of different satellite radiance instruments in a thinning box. Discussions with EMC lead to the suggestion to turn dval=0 for all radiance data types so no specific types are unequally weighted during the thinning processing (therefore increasing the CrIS usage). EMC plans to remove 'dval' option in the near future; so removing this option by setting 'dval' to 0 will eliminate future issues.

3. Sensitivity tests on traditional and non-traditional observation sources

a. Motivation/Background

Sensitivity tests on regional scale model runs were preformed for the Air Force in order to assist with data and system configuration that optimize the use of new and proposed source of data for GSI. The FY2014 SOW states the DTC must perform sensitivity tests on at least 2 types from the following list:

- GCOM-W1 AMSR2
- NPP CrIS
- NOAA-16/18/19 SBUV/2
- METOP-A GOME-2

The GCOM-W1 AMSR2 was eliminated from the list after DTC confirmed with the Joint Center for Satellite Data Assimilation (JCSDA) and NCEP EMC colleagues that this data type was not yet available for ingest into GSI and would not be ready within the period of performance. It was agreed upon to skip this data type during the mid-term review in August, 2014.

b. Experiment design

i. System

The setup of the DTC end-to-end data assimilation and forecasting system followed the workflow provided by the Air Force. The only major differences between the Air Force system and the DTC system is the background and boundary conditions for the DTC system come from the GFS, whereas the Air Force uses the UKMET. This year the DTC updated the end-to-end system to use all Air Force observation data, with the exception of the SBUV and GOME data, which are not currently used for Air Force operations. These data were obtained from the NCEP BUFR files.

The DTC system, shown in Figure 2.b-i.1, includes two cycles, a 06 UTC cold start cycle and a 12 UTC continuous cycle. The 06 UTC cold start cycle starts with collecting background files, GFS 0-56 hour forecasts initiated at 06 UTC (GRIB2 files, 0.5° horizontal resolution) from NCEP and NavySST data from Air Force archives. The WRF preprocessing system (WPS and *real*) is then run to decode and interpolate data into the testing domain and grids. *real* is run twice; first to generate a background file for GSI, wrf_input, valid at 06 UTC (GFS analysis) and boundary conditions valid from 06-12 UTC, and a second time to generate the boundary files covering 48 hour forecasts starting from 12 UTC. Next, GSI is run to generate an analysis using the background from the 06 UTC GFS analysis and the observations within a ±3 hour time window from the Air Force PrepBUFR (for conventional observations) and BUFR files (for satellite observations). For satellite data assimilation, GSI cycles the radiance bias correction by reading the radiance bias correction coefficients from the previous GSI cycle. The bias correction coefficients are then updated for angular bias correction. The boundary conditions are then updated by *update_BC* using the GSI analyses and GFS forecasts. Finally, ARW is run to generate 6 hour model forecasts. Unlike the 06 UTC cycle, the 12 UTC continuous cycle uses the 6 hour forecasts generated by the 06 UTC cycle as the background. Following the GSI run, ARW is run to produce 48 hour forecasts for verification. The 06 UTC cold start and subsequent 12 UTC continuous cycle is then repeated with a 18 UTC cold start and 00 UTC continuous cycle. The forecasts are processed by the UPP system and verified by the Model Evaluation Tools (MET) against GFS PrepBUFR conventional data and the ERA-interim reanalysis dataset (regridded to match WRF).

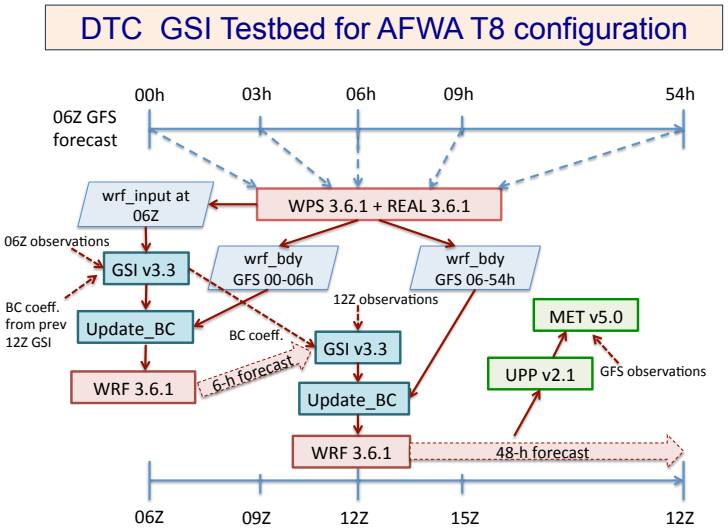

Figure 2.b-i.1: Schematic of DTC end-to-end data assimilation and forecast system following the Air Force pre-operational configuration.

The versions of model components of the system are listed as follows:

- GSI: v3.3
- update_BC: 2014 version
- WRF: v3.6.1
- UPP: v2.1

- MET: v5.0

Appendix A provides relevant portions of the GSI namelist used in the DTC system.
Appendix B provides relevant portions of the ARW namelist used in the DTC system.

ii. Data

Table 3.b-ii.1 summarizes the data linked, read into, and used in the analysis for both the DTC and Air Force systems. When building the DTC GSI configuration, channels and prepBUFR observation types followed those of the Air Force system by matching convinfo and satinfo files.

Table 3.b-ii.1: Data assimilated for data impact experiments

	Observations assimilated
Conventional	Air Force Prepbufr conventional observations
	GPS RO
Satellite radiances	AMSU-A (noaa-15, -18, -19, metop-a, -b, aqua)
	ATMS (npp)
	HIRS4 (noaa-19, metop-a, -b)
	AIRS (aqua)
	MHS (noaa-18, -19, metop-a, -b)
	IASI (metop-a, -b)
	CRIS (npp)*
Ozone **	SBUV/2 (noaa-17,-18,-19)
	GOME (metop-a, -b)

*npp CrIS included in control configuration, excluded for CrIS data denial run
** ozone types only assimilated for ozone-impact runs

iii. Domains

Due to specific interest in the regional domains, the Caribbean (also known as T8) domain was chosen for the FY2014 DTC testing. The domain is pictured in Figure 2.b-iii.1. The 212x122 grid is configured with a 15 km horizontal resolution. The operational configuration uses 57 full vertical sigma levels with a 10 hPa model top, however in order to properly test ozone, the number of vertical sigma levels was increased to 62 with a 2 hPa model top. Results comparing the 10 hPa to the 2 hPa model top in the T8 domain are described in section c.

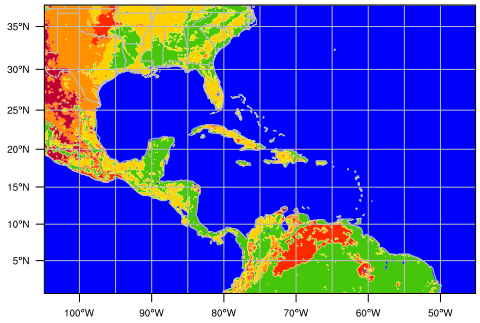

Figure 2.b-iii.1: Air Force Caribbean (T8) domain used for DTC model top comparison test.

While configuring the model and GSI for the data impact experiments, it was noted that the data types of interest were not present in the T8 domain due to the timing of the satellite overpasses. In order to capture the overpasses during 00 UTC and/or 12 UTC initializations, the T8 domain was "shifted" to the Eastern North Pacific for NPP (CrIS) and noaa-19 (SBUV) coverage and to the Atlantic Basin for Metop-a and Metop-b (GOME) coverage. Due to a relatively large map factor values near to northern edge of the domain, the T8 configuration was altered slightly to add a few extra longitude grid-points and a few fewer latitude grid-points. The resulting domains are pictured in Figure 2.b-iii.2.

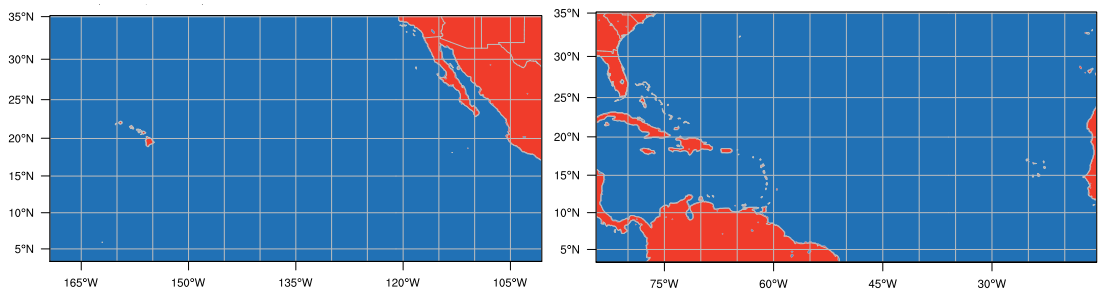

Figure 2.b-iii.2: Eastern Pacific (left) and Atlantic Basin (right) domains used for DTC data impact tests.

c. Model top test

A model top test was performed in order to assess whether raising the model top from 10 hPa to 2 hPa, as requested by Air Force for the purpose of the data impact tests would provide an improvement, degradation, or neutral results relative to the current operational configuration at 10 hPa. A few additional changes needed to be made in order to raise the model top, including increasing the vertical sigma levels from 57 to 62, changing the lapse rate profile in the stratosphere and other namelist changes as recommended by NCAR Mesoscale & Microscale Meteorology Division (MMM) ARW developers (see Appendix B for namelist). As a result, the ARW version used for the tests was v3.6.1, which include the proper modifications for the stratospheric lapse rate. Finally, the Air Force operational radiation schemes were changed from rrtm (longwave) and dudia (shortwave) to the rrtmg (for both longwave and shortwave) to accommodate the increased model top.

i. GSI diagnostics

The analysis increment and innovation before and after bias correction was investigated for higher peaking (channel 9 and 10) AMSU-A channels assimilated into both the 10 hPa and 2 hPa experiments. The same channel selection (following the operational configuration) was used for both runs. However, due to the increase of the model top, additional radiance data were assimilated for the 2 hPa experiment. Figure 2.c-i.1 shows the increments for each cycle for both channel 9 and 10. Overall, the 2 hPa shows a smaller bias in both O-A and O-B statistics with a clear improvement over the 10 hPa experiment for channel 10.

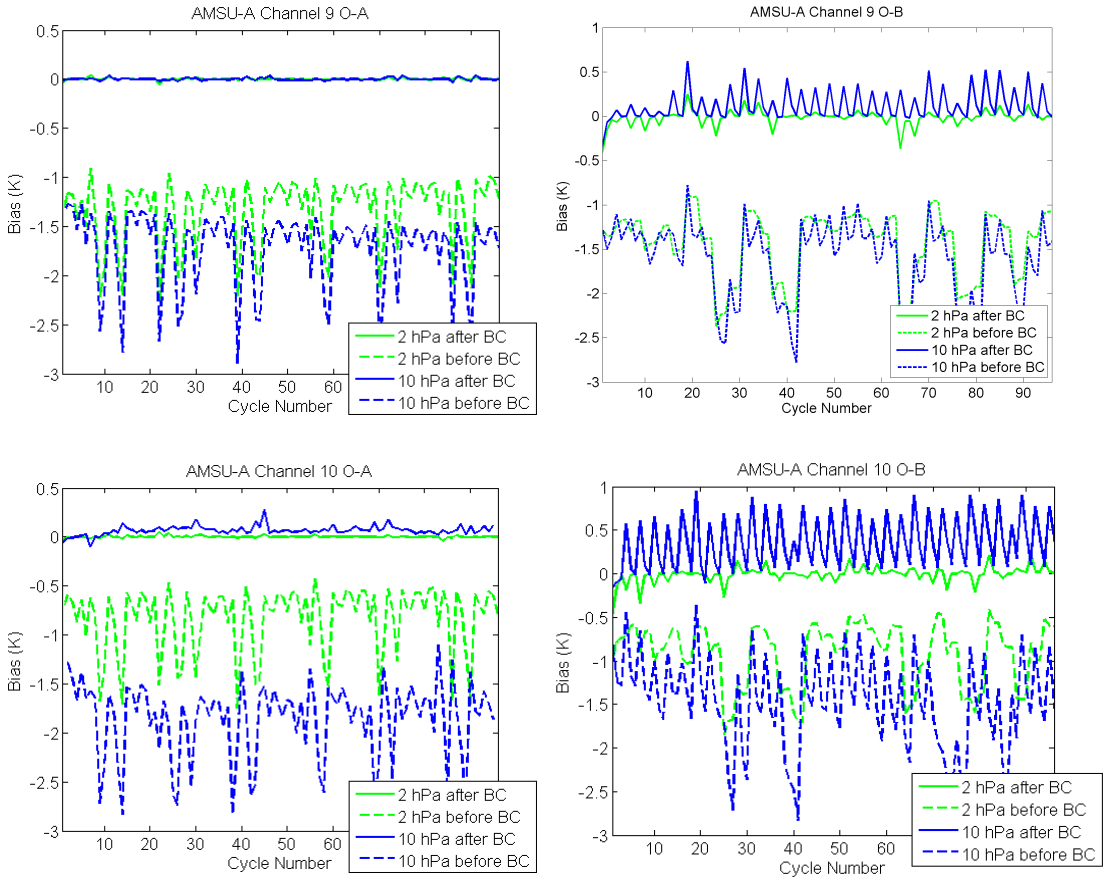

Figure 2.c-i.1: O-A (left) and O-B (right) for AMSU-A channel 9 (top) and channel 10 (lower). Comparison of 10 hPa model top (blue) before (dashed) and after bias correction (solid) and 2 hPa model top (green) before (dashed) and after (solid) bias correction.

ii. Verification against ERA-I

Verification against the ERA-interim reanalysis was performed and pairwise differences were computed to determine whether one configuration was statistically significantly (SS) outperforming the other configuration. Table 2.c-ii.1 shows the summary table of bias, whereas Table 2.c-ii.2 shows the summary table for RMSE for temperature, zonal wind, meridional wind, and specific humidity. The cell is shaded green when the 2 hPa model top configuration was SS better and shaded blue when the 10 hPa model top

configuration was SS better. The bias statistics show mixing results, while the RMSE statistics favor the 2 hPa model top test.consistently for different variables.

Table 2.c-ii.1: Statistical Significance table for model top test biases.

99% CI Statistical Significance Table (bias): CTL02 vs. CTL10

TEMP Bias		Forecast Lead Time (hr)								
		0	6	12	18	24	30	36	42	48
Pressure Levels (hPa)	50	CTRL	--	CTRL	EXPT	CTRL	CTRL	--	CTRL	--
	100	EXPT	EXPT	EXPT	CTRL	CTRL	CTRL	CTRL	CTRL	CTRL
	250	EXPT	EXPT	EXPT	EXPT	--	--	--	--	CTRL
	400	CTRL	CTRL	CTRL	CTRL	CTRL	CTRL	CTRL	CTRL	CTRL
	500	--	EXPT	EXPT	EXPT	EXPT	EXPT	EXPT	EXPT	EXPT
	700	CTRL	EXPT	EXPT	EXPT	EXPT	EXPT	EXPT	EXPT	EXPT
	850	EXPT	EXPT	EXPT	EXPT	EXPT	EXPT	EXPT	EXPT	EXPT
	925	EXPT	EXPT	EXPT	EXPT	EXPT	EXPT	EXPT	EXPT	CTRL

U-Wind Bias		Forecast Lead Time (hr)								
		0	6	12	18	24	30	36	42	48
Pressure Levels (hPa)	50	EXPT	--	EXPT	EXPT	EXPT	--	EXPT	EXPT	--
	100	--	CTRL	CTRL	CTRL	CTRL	CTRL	CTRL	CTRL	CTRL
	250	--	CTRL	CTRL	--	--	--	EXPT	EXPT	EXPT
	400	CTRL	CTRL	CTRL	CTRL	CTRL	EXPT	EXPT	EXPT	EXPT
	500	CTRL	CTRL	CTRL	CTRL	CTRL	CTRL	EXPT	EXPT	EXPT
	700	CTRL	CTRL	EXPT	EXPT	CTRL	CTRL	CTRL	CTRL	CTRL
	850	CTRL	--	EXPT	EXPT	--	--	--	CTRL	CTRL
	925	CTRL	CTRL	--	EXPT	--	--	--	EXPT	EXPT

V-Wind Bias		Forecast Lead Time (hr)								
		0	6	12	18	24	30	36	42	48
Pressure Levels (hPa)	50	--	CTRL	--	CTRL	CTRL	EXPT	--	CTRL	CTRL
	100	EXPT	CTRL	--	CTRL	EXPT	--	CTRL	--	CTRL
	250	--	--	--	--	--	EXPT	EXPT	EXPT	EXPT
	400	CTRL	CTRL	EXPT	EXPT	EXPT	EXPT	EXPT	--	EXPT
	500	CTRL	CTRL	EXPT	EXPT	EXPT	EXPT	--	--	EXPT
	700	CTRL	CTRL	CTRL	CTRL	CTRL	CTRL	--	CTRL	CTRL
	850	CTRL	CTRL	--	--	--	CTRL	CTRL	--	--
	925	EXPT	--	--	EXPT	EXPT	EXPT	EXPT	EXPT	EXPT

SPFH Bias		Forecast Lead Time (hr)								
		0	6	12	18	24	30	36	42	48
Pressure Levels (hPa)	50	--	--	--	--	--	--	--	--	--
	100	--	--	--	--	--	--	--	--	--
	250	CTRL	CTRL	CTRL	EXPT	EXPT	EXPT	EXPT	EXPT	EXPT
	400	EXPT	EXPT	EXPT	EXPT	EXPT	EXPT	EXPT	EXPT	EXPT
	500	EXPT	EXPT	EXPT	EXPT	EXPT	EXPT	EXPT	EXPT	EXPT
	700	EXPT	EXPT	EXPT	EXPT	EXPT	EXPT	EXPT	EXPT	EXPT
	850	EXPT	--	CTRL	CTRL	CTRL	CTRL	CTRL	CTRL	CTRL
	925	CTRL	CTRL	EXPT	EXPT	EXPT	EXPT	EXPT	EXPT	EXPT

Table 2.c-ii.2: same as Table 2.c-ii.1 except RMSE statistics

99% CI Statistical Significance Table (RMSE): CTL02 vs. CTL10

TEMP RMSE		Forecast Lead Time (hr)								
		0	6	12	18	24	30	36	42	48
Pressure Levels (hPa)	50	--	EXPT	EXPT	EXPT	EXPT	EXPT	EXPT	EXPT	EXPT
	100	EXPT	EXPT	EXPT	EXPT	--	--	--	--	--
	250	EXPT	EXPT	EXPT	EXPT	EXPT	EXPT	EXPT	--	EXPT
	400	--	CTRL	CTRL	CTRL	CTRL	CTRL	CTRL	CTRL	CTRL
	500	CTRL	--	EXPT	EXPT	EXPT	EXPT	EXPT	EXPT	EXPT
	700	CTRL	--	EXPT	EXPT	EXPT	EXPT	EXPT	EXPT	EXPT
	850	EXPT	EXPT	EXPT	EXPT	EXPT	EXPT	EXPT	EXPT	EXPT
	925	EXPT	EXPT	EXPT	EXPT	EXPT	EXPT	EXPT	EXPT	EXPT

U-Wind RMSE		Forecast Lead Time (hr)								
		0	6	12	18	24	30	36	42	48
Pressure Levels (hPa)	50	EXPT	EXPT	EXPT	EXPT	--	EXPT	EXPT	EXPT	--
	100	--	CTRL	CTRL	CTRL	--	--	--	--	--
	250	EXPT	EXPT	EXPT	EXPT	--	--	EXPT	EXPT	EXPT
	400	--	CTRL	--	--	EXPT	EXPT	EXPT	EXPT	EXPT
	500	--	CTRL	--	--	EXPT	EXPT	EXPT	EXPT	EXPT
	700	--	CTRL	--	--	--	--	EXPT	EXPT	EXPT
	850	EXPT	CTRL	--	EXPT	--	--	--	EXPT	EXPT
	925	EXPT	CTRL	--	EXPT	--	--	EXPT	EXPT	EXPT

V-Wind RMSE		Forecast Lead Time (hr)								
		0	6	12	18	24	30	36	42	48
Pressure Levels (hPa)	50	EXPT	EXPT	EXPT	EXPT	EXPT	EXPT	EXPT	EXPT	EXPT
	100	EXPT	EXPT	EXPT	EXPT	EXPT	EXPT	EXPT	EXPT	EXPT
	250	EXPT	EXPT	--	--	--	--	--	--	--
	400	EXPT	--	--	--	--	EXPT	--	--	--
	500	--	CTRL	--	CTRL	--	--	CTRL	CTRL	--
	700	--	--	EXPT	--	EXPT	--	EXPT	--	EXPT
	850	--	EXPT	EXPT	--	EXPT	--	--	--	--
	925	--	EXPT	EXPT	EXPT	EXPT	EXPT	EXPT	EXPT	EXPT

SPFH RMSE		Forecast Lead Time (hr)								
		0	6	12	18	24	30	36	42	48
Pressure Levels (hPa)	50	--	--	--	--	--	--	--	--	--
	100	--	--	--	--	--	--	--	--	--
	250	CTRL	--	EXPT	EXPT	EXPT	EXPT	EXPT	EXPT	--
	400	EXPT	--	EXPT	EXPT	EXPT	EXPT	EXPT	EXPT	EXPT
	500	EXPT	--	--	--	--	EXPT	EXPT	EXPT	EXPT
	700	EXPT	EXPT	EXPT	--	EXPT	--	EXPT	EXPT	EXPT
	850	EXPT	CTRL	CTRL	CTRL	CTRL	CTRL	CTRL	CTRL	CTRL
	925	CTRL	CTRL	CTRL	CTRL	CTRL	CTRL	CTRL	CTRL	CTRL

Due to the large number of points used for the grid-based verification, a large number of SS differences were found. Consideration of the magnitude of the difference should provide some added information as to what SS differences are most meaningful. Vertical profiles for temperature (Figure 2.c-ii.1) at 12- and 48-hour forecast times show large improvements at the shorter lead times favoring the 2 hPa model top above 250 hPa and below 850 hPa. At the 48-hour forecast time, the SS test still shows nearly all levels in favor of the 2 hPa model top, however the magnitude of the differences are clearly smaller.

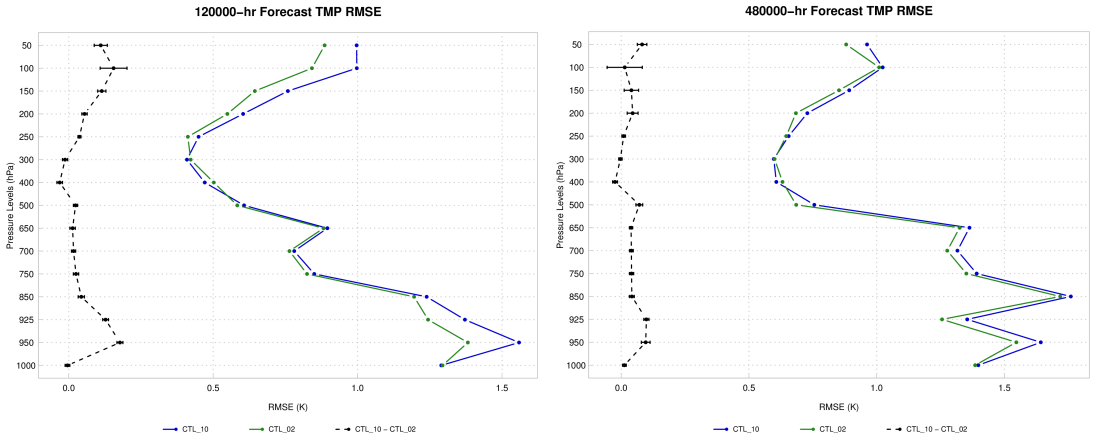

Figure 2.c-ii.1: Vertical profile for 12 (left) and 48 (right) hour forecast temperature RMSE. Comparison of model top test with 2 hPa model top in green and 10 hPa model top in blue. The pairwise difference is indicated by the black dashed like, where the difference is SS if the confidence intervals do not encompass zero. SS determined at the 99% level.

Figure 2.c-ii.2 shows a time series for temperature (RMSE) for 150 and 500 hPa, which show that the SS improvement in the temperature field for the 2 hPa model top configuration is fairly consistent for the entire forecast period.

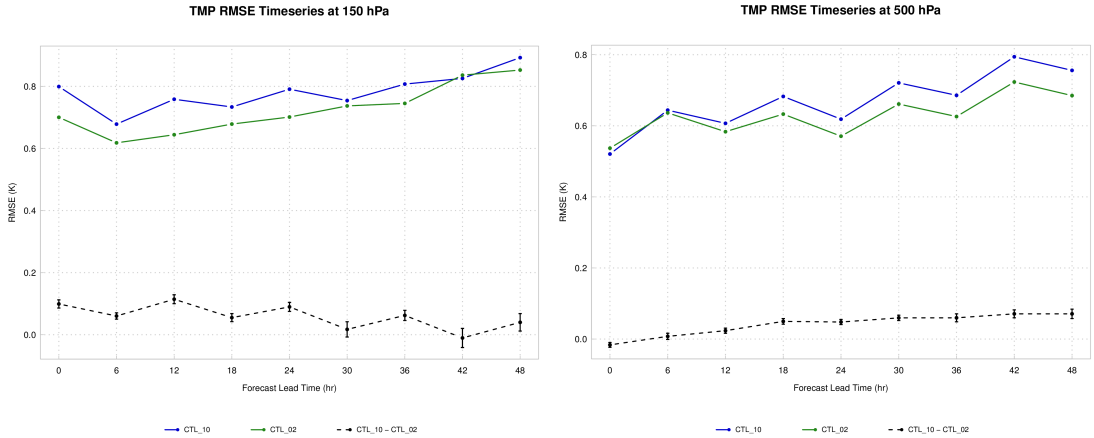

Figure 2.c-ii.2: Timeseries of temperature RMSE at 150 hPa (left) and 500 hPa (right). Same configuration and notations as Figure 2.c-ii.1.

The wind field (Figure 2.c-ii.3) shows consistent SS improvement in favor of the 2 hPa configuration, however the larger differences between the configurations seem to be limited to the upper levels (above 250 hPa), with fewer SS differences between the configurations at longer lead times.

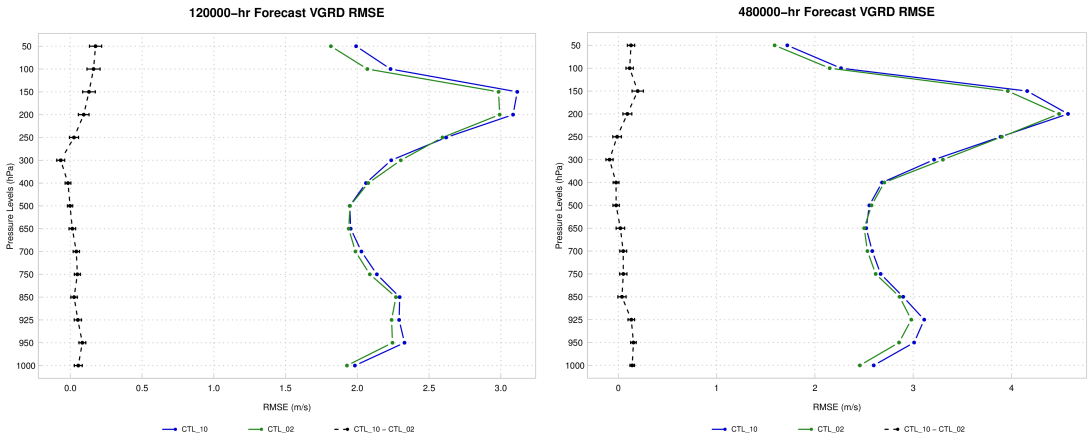

Figure 2.c-ii.3: same as Figure 2.c-ii.1 except v-component wind.

Opposite to the v-component wind, the u-component (Figure 2.c-ii.4) shows SS differences isolated at the longer lead times (beyond 30 hours).

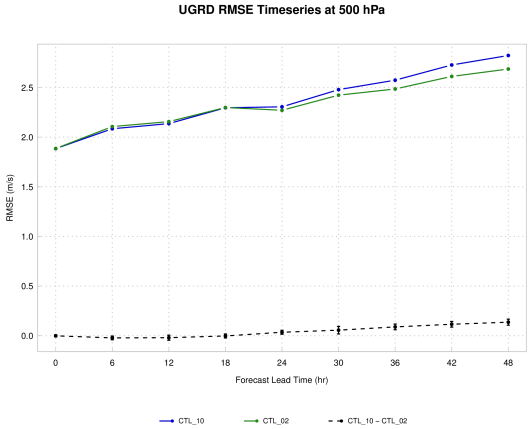

Figure 2.c-ii.4: same as Figure 2.c-ii.2 except u-component wind at 500 hPa.

Figure 2.c-ii.5 demonstrates that although there are many SS differences shown in the tables for the SPFH field, many of these differences are very small and do not grow through the forecast period.

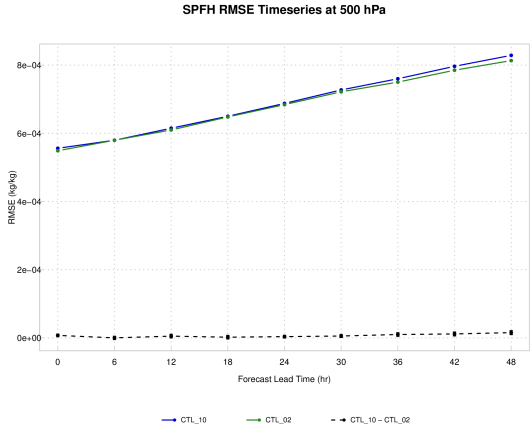

Figure 2.c-ii.5: same as Figure 2.c-ii.2 except specific humidity at 500 hPa.

Figure 2.c-ii.6 examines the biases and characteristics of the two model runs relative to ERA-I. For 150 hPa temperature biases, the 2 hPa model top experiment shows warmer temperatures relative to ERA-I off the southeastern coast of the U.S., but is predominately characterized by the less cool (relative to ERA-I) temperatures over the gulf of Mexico and Caribbean. Although both runs are cooler than ERA-I, the 10 hPa model top run shows much cooler temperatures than the 2 hPa model top run. When considering the mid-level zonal winds (500 hPa), the predominate difference between the two runs is the presence of more westerly winds in the 10 hPa model top run relative to ERA-I than the 2 hPa model top run. Finally, as shown in Figure 2.c-ii.5, the specific humidity differences between the 2 hPa and 10 hPa model top runs are fairly neutral with no clear differences in the biases.

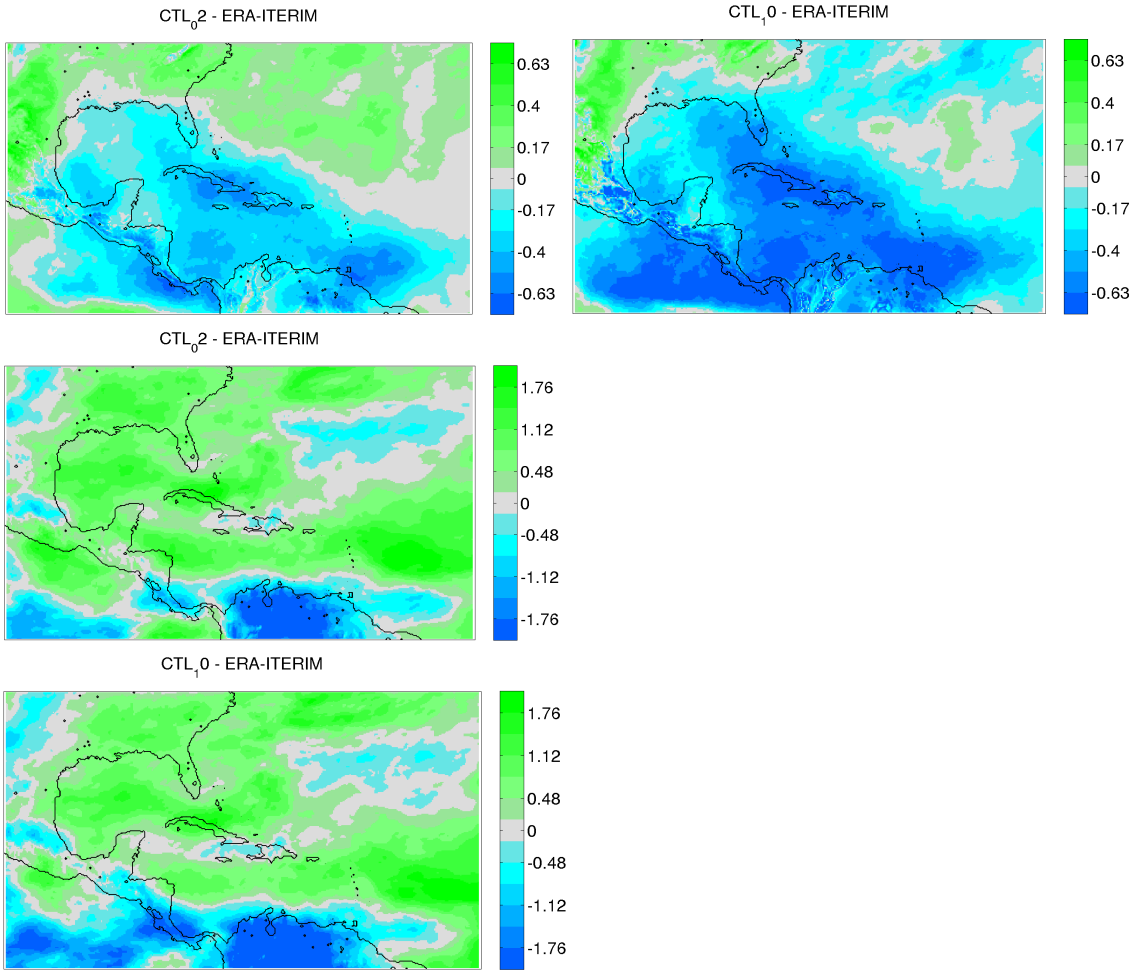

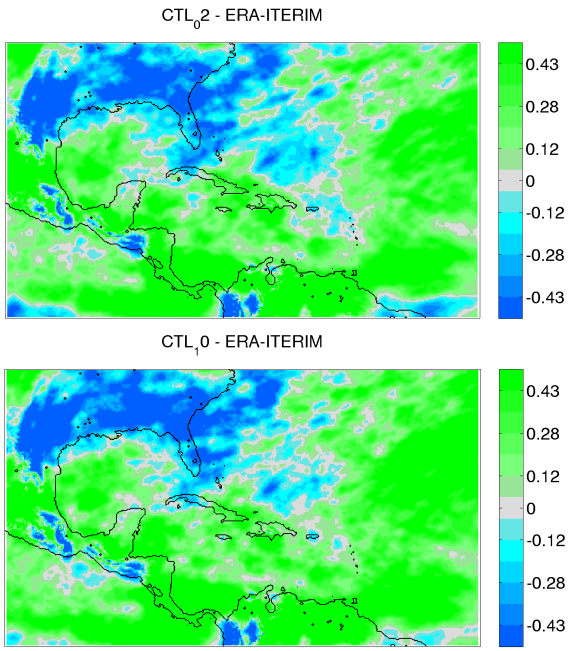

Figure 2.c-ii.6: 24-hours forecast biases between the 2 hPa (left) and 10 hPa (right) model top configuration and ERA-I for 150 hPa temperature (top), 500 hPa zonal winds (center), and 700 hPa specific humidity (lower).

d. Ozone data impact

i. SBUV/2

SBUV profile ozone was assimilated into GSI to explore the use of ozone data in GSI with ARW for regional applications. It is important to note that ARW does not have ozone as a prognostic variable; therefore the data impact tests present indirect effects of the ozone assimilation on the analysis via the radiation changes in the CRTM calculation. In order to have background ozone for GSI to increment, the GFS ozone was read in by GSI and interpolated to the regional domain. Because the SBUV sensor only records one time per day, the 00 UTC initializations only were aggregated for verification to isolate the impact of the SBUV data.

The SS tables 2.d-i.2.1 and 2.d-i.2.2 show a signal of SS improvement when assimilating SBUV ozone in upper level temperature for both bias and RMSE, early lead time improvements in RMSE for the wind fields throughout the vertical levels, and mixed improvement/degradations for both bias and RMSE for specific humidity.

Table 2.d-i.2.1: same as Table 2.c-ii.1 except comparison between SBUV (green) assimilation and control configuration (blue; following Air Force operational configuration).

99% CI Statistical Significance Table (bias): SBUV vs. CTL02 (EPAC)

TEMP Bias		Forecast Lead Time (hr)								
		0	6	12	18	24	30	36	42	48
Pressure Levels (hPa)	50	EXPT	EXPT	--	EXPT	CTRL	EXPT	--	--	--
	100	EXPT	CTRL	CTRL	CTRL	CTRL	CTRL	CTRL	CTRL	CTRL
	250	--	CTRL	CTRL	CTRL	CTRL	CTRL	CTRL	CTRL	CTRL
	400	--	EXPT	EXPT	EXPT	EXPT	EXPT	EXPT	EXPT	EXPT
	500	--	--	--	--	--	--	--	EXPT	EXPT
	700	EXPT	--	--	--	--	--	--	--	--
	850	EXPT	--	CTRL	--	--	--	--	--	--
	925	EXPT	--	--	--	--	--	--	--	--

U-Wind Bias		Forecast Lead Time (hr)								
		0	6	12	18	24	30	36	42	48
Pressure Levels (hPa)	50	EXPT	CTRL	--	EXPT	EXPT	EXPT	EXPT	EXPT	EXPT
	100	--	CTRL	--	--	CTRL	--	CTRL	EXPT	--
	250	CTRL	CTRL	CTRL	CTRL	CTRL	CTRL	CTRL	--	--
	400	CTRL	EXPT	EXPT	EXPT	--	--	CTRL	CTRL	CTRL
	500	CTRL	EXPT	EXPT	EXPT	EXPT	--	CTRL	EXPT	CTRL
	700	--	EXPT	--	CTRL	--	EXPT	EXPT	EXPT	--
	850	--	--	CTRL	CTRL	CTRL	EXPT	EXPT	--	CTRL
	925	CTRL	--	EXPT	EXPT	EXPT	--	--	--	CTRL

V-Wind Bias		Forecast Lead Time (hr)								
		0	6	12	18	24	30	36	42	48
Pressure Levels (hPa)	50	--	--	EXPT	CTRL	EXPT	CTRL	CTRL	CTRL	CTRL
	100	--	--	--	EXPT	--	CTRL	CTRL	--	--
	250	--	CTRL	EXPT	--	EXPT	EXPT	--	CTRL	EXPT
	400	--	--	--	--	EXPT	EXPT	--	CTRL	CTRL
	500	--	EXPT	--	--	EXPT	CTRL	--	CTRL	CTRL
	700	EXPT	--	EXPT	CTRL	CTRL	EXPT	--	--	--
	850	--	--	EXPT	CTRL	EXPT	EXPT	EXPT	--	--
	925	--	CTRL	EXPT	--	EXPT	EXPT	EXPT	--	EXPT

SPFH Bias		Forecast Lead Time (hr)								
		0	6	12	18	24	30	36	42	48
Pressure Levels (hPa)	50	--	--	--	--	--	--	--	--	--
	100	--	--	--	--	--	--	--	--	--
	250	EXPT	EXPT	EXPT	CTRL	CTRL	CTRL	--	CTRL	CTRL
	400	--	--	--	--	--	EXPT	EXPT	EXPT	EXPT
	500	--	--	--	--	--	--	--	--	EXPT
	700	--	--	--	--	--	--	--	--	--
	850	CTRL	CTRL	CTRL	CTRL	CTRL	CTRL	CTRL	CTRL	CTRL
	925	--	--	--	CTRL	CTRL	CTRL	CTRL	CTRL	CTRL

Table 2.d-i.2.2: same as Table 2.d-i.2.1 except RMSE statistics.

99% CI Statistical Significance Table: SBUV vs. CTL02 (EPAC)

TEMP RMSE		Forecast Lead Time (hr)								
		0	6	12	18	24	30	36	42	48
Pressure Levels (hPa)	50	EXPT	EXPT	EXPT	EXPT	EXPT	EXPT	EXPT	EXPT	--
	100	EXPT	--	--	--	--	CTRL	--	--	--
	250	--	--	--	CTRL	CTRL	CTRL	CTRL	CTRL	CTRL
	400	--	EXPT	EXPT	--	--	--	EXPT	--	--
	500	--	EXPT	EXPT	EXPT	EXPT	EXPT	EXPT	EXPT	EXPT
	700	--	--	--	--	--	--	--	--	--
	850	--	--	--	--	--	--	--	--	--
	925	EXPT	--	--	--	--	CTRL	CTRL	--	--

U-Wind RMSE		Forecast Lead Time (hr)								
		0	6	12	18	24	30	36	42	48
Pressure Levels (hPa)	50	EXPT	EXPT	EXPT	EXPT	EXPT	EXPT	--	EXPT	EXPT
	100	EXPT	EXPT	--	--	CTRL	--	--	--	--
	250	--	--	--	--	--	CTRL	--	--	--
	400	EXPT	EXPT	EXPT	EXPT	EXPT	--	--	--	--
	500	EXPT	--	EXPT	EXPT	--	--	CTRL	--	--
	700	--	EXPT	EXPT	EXPT	--	--	--	--	--
	850	EXPT	EXPT	--	--	--	--	--	--	--
	925	CTRL	EXPT	EXPT	EXPT	--	--	--	--	--

V-Wind RMSE		Forecast Lead Time (hr)								
		0	6	12	18	24	30	36	42	48
Pressure Levels (hPa)	50	EXPT	EXPT	EXPT	EXPT	EXPT	EXPT	EXPT	--	EXPT
	100	EXPT	--	--	--	--	--	--	--	--
	250	--	EXPT	EXPT	--	--	--	--	--	--
	400	EXPT	EXPT	EXPT	EXPT	--	--	--	--	--
	500	EXPT	EXPT	EXPT	--	--	--	--	--	--
	700	EXPT	EXPT	EXPT	EXPT	--	--	--	--	--
	850	EXPT	--	--	--	--	EXPT	--	--	--
	925	--	EXPT	EXPT	--	--	EXPT	--	--	--

SPFH RMSE		Forecast Lead Time (hr)								
		0	6	12	18	24	30	36	42	48
Pressure Levels (hPa)	50	--	--	--	--	--	--	--	--	--
	100	--	--	--	--	--	--	--	--	--
	250	--	--	--	--	--	CTRL	--	CTRL	--
	400	CTRL	--	EXPT	EXPT	EXPT	--	--	--	--
	500	--	CTRL	--	--	EXPT	EXPT	EXPT	EXPT	--
	700	--	--	--	--	--	--	EXPT	--	--
	850	--	--	--	CTRL	CTRL	CTRL	CTRL	CTRL	CTRL
	925	--	--	--	CTRL	CTRL	CTRL	CTRL	CTRL	CTRL

Figure 2.d-i.2.1 shows large consistent SS improvement in the analysis temperature for the SBUV assimilation over the control run with differences still present in the mid- and upper-levels out to 12 hours, with differences fading by the 36-hour forecast time.

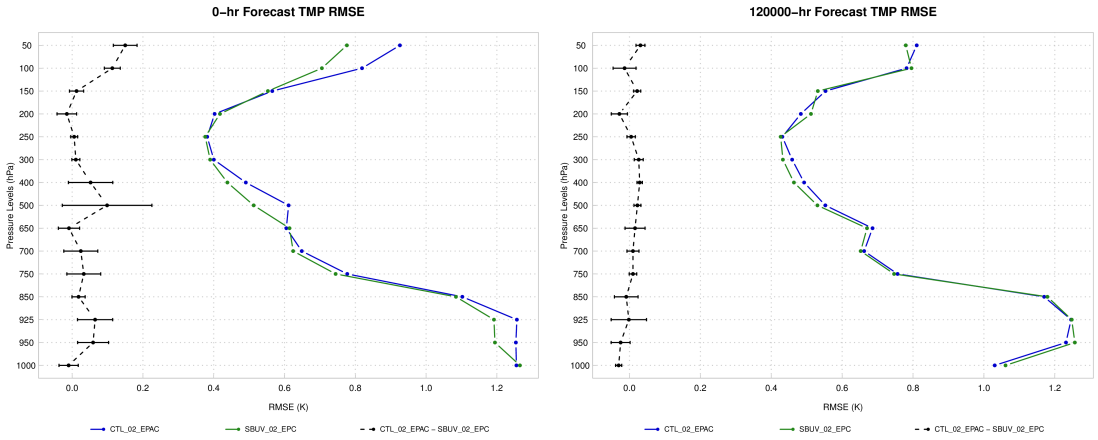

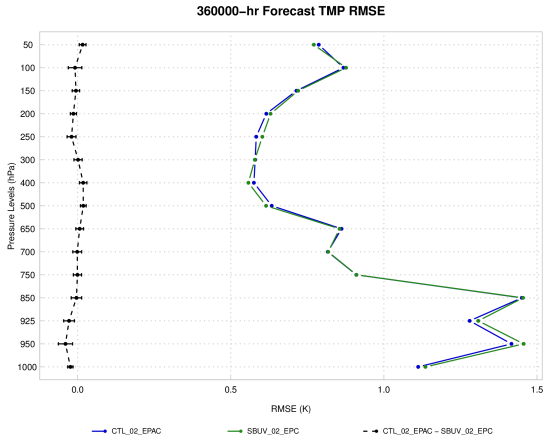

Figure 2.d-i.2.1: Vertical profile of temperature RMSE at 0 (upper left), 12 (upper right), and 36-hour (lower left) forecast lead time. Pairwise differences between the SBUV assimilation configuration (green), control configuration (blue) are indicated in black. The difference is SS different with the CI does not encompass zero.

The taper in the magnitude of the SS differences with lead time is apparent in Figure 2.d-i.2.2, for 50 hPa and 500 hPa temperature. Differences converge around 18 hours with small SS differences remaining throughout the forecast period.

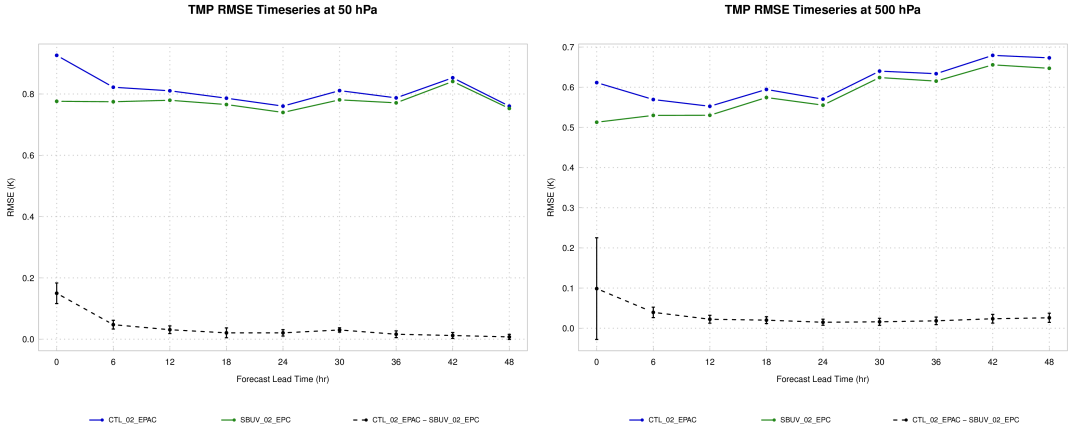

Figure 2.d-i.2.2: Same as Figure 2.d-i.2.1 except timeseries for 50 hPa temperature (left) and 500 hPa temperature (right).

Biases for each of the configurations relative to ERA-I are shown in Figure 2.d-i.2.3. Notable differences between the runs occur around the Yucatan Peninsula, where warmer temperatures relative to the SBUV ozone assimilation run characterize the control configuration. The pairwise differences between the two runs relative to ERA-I were computed for each grid point, where differences favoring the SBUV configuration are hatched in red and differences favoring the control configuration are hatched in black. Differences in the target region show spatially coherent SS differences favoring the SBUV configuration.

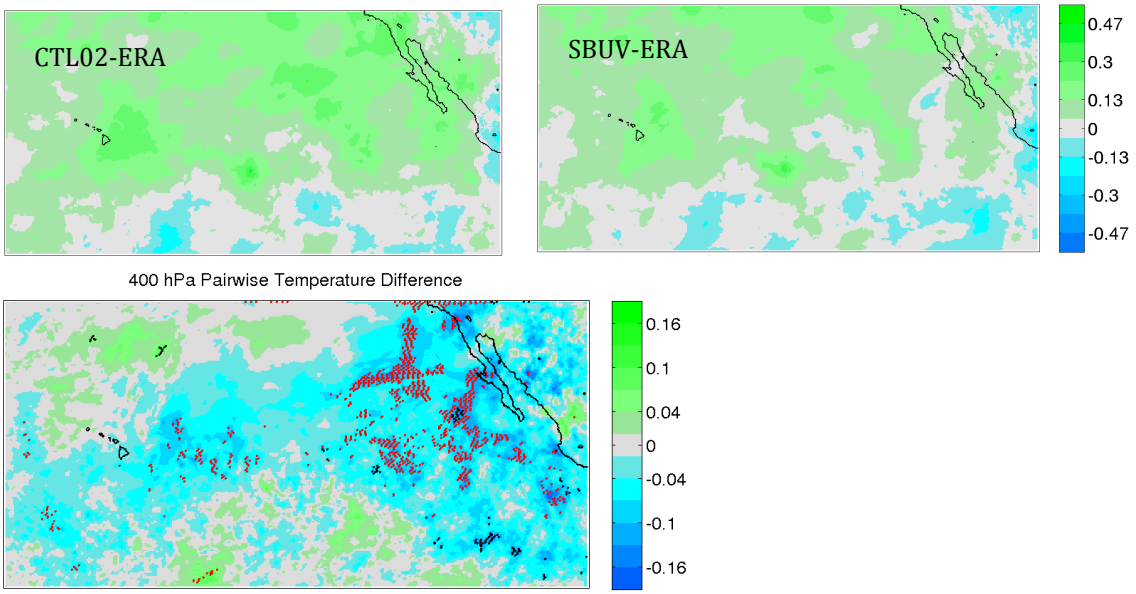

Figure 2.d-i.2.3: 12-hour forecast biases for 400 hPa temperature differences between the control run (left) and the SBUV assimilation run (right) and ERA-I. Spatial pairwise SS differences were computed between the two configurations, where the SS differences favoring the SBUV assimilation are indicated with red hatching and SS differences favoring the control configuration are indicated with black hatching.

Figure 2.d-i.2.4 shows differences in the v-component wind field. Most of SS differences favors the SBUV assimilation configuration with a stronger signal of improvement at the 12-hour forecast time. Small SS differences favoring the control run are isolated to the upper-most vertical levels at 36-hours.

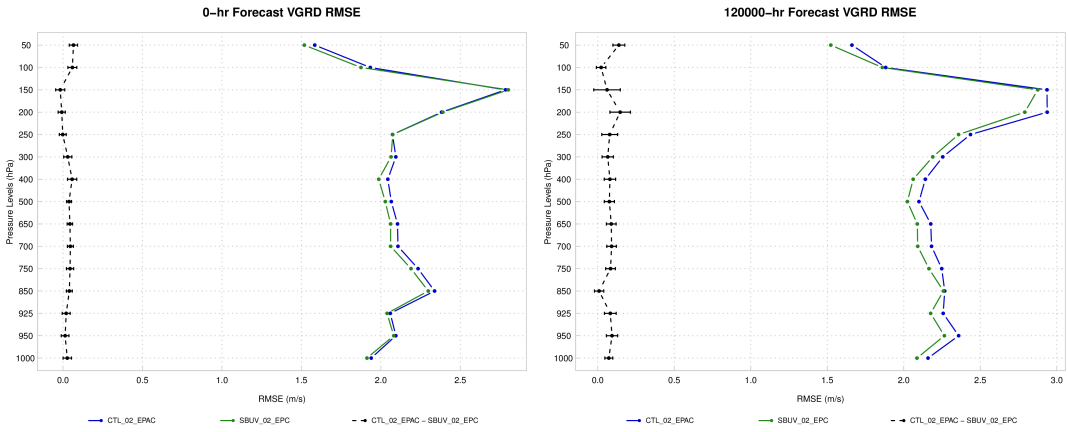

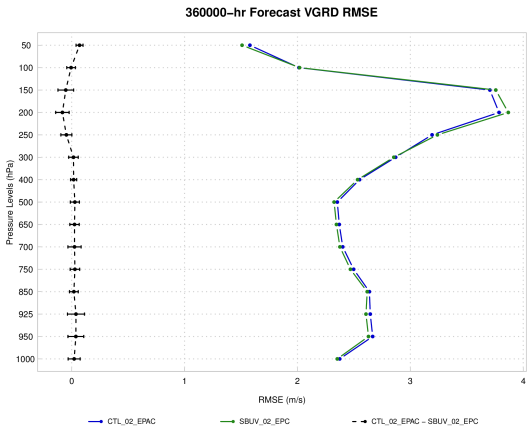

Figure 2.d-i.2.4: same as 2d-i.2.1 except v-component wind RMSE.

Figure 2.d-i.2.5 shows, as with temperature, that the larger impacts are more prevalent in the earlier lead times (out to 24-30 hours for u-component wind). SS differences are most notable in the upper levels (50 hPa), with smaller magnitude SS differences occurring at mid-levels (500 hPa).

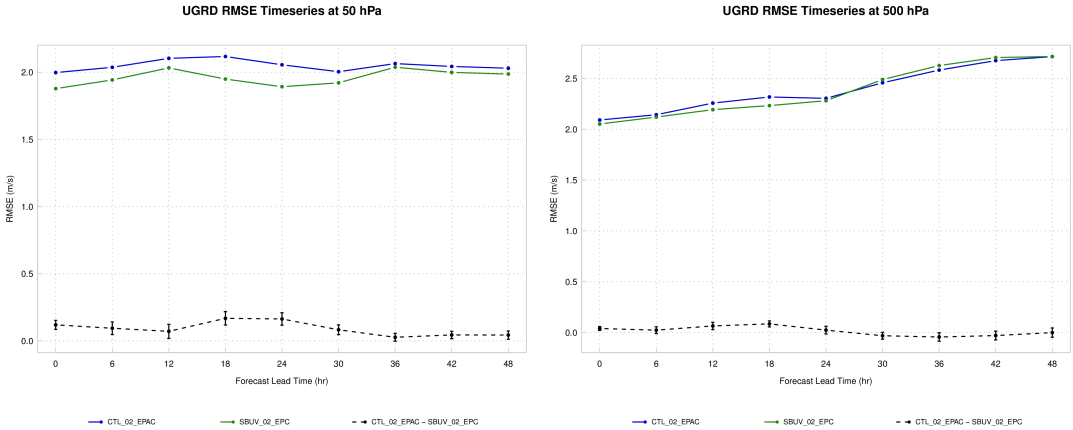

Figure 2.d-i.2.5: same as 2.d-i.2.2 except u-component wind RMSE at 50 hPa (left) and 500 hPa (right).

Zonal wind biases at 50 hPa for each configuration relative to ERA-I are show in Figure 2.d-i.2.6, where differences show more westerly winds in the control configuration relative to ERA-I in the north-central portion of the domain and more easterly winds in the southeastern portion of the domain. Conversely, the SBUV configuration has a strong area of increased westerly winds in the southwestern portion of the domain. When considering the pairwise differences between these two configurations for each grid-point, the SBUV configuration has numerous regions of SS differences in favor of the SBUV configuration, with a pocket of degradations associated with the previously mentioned westerly winds.

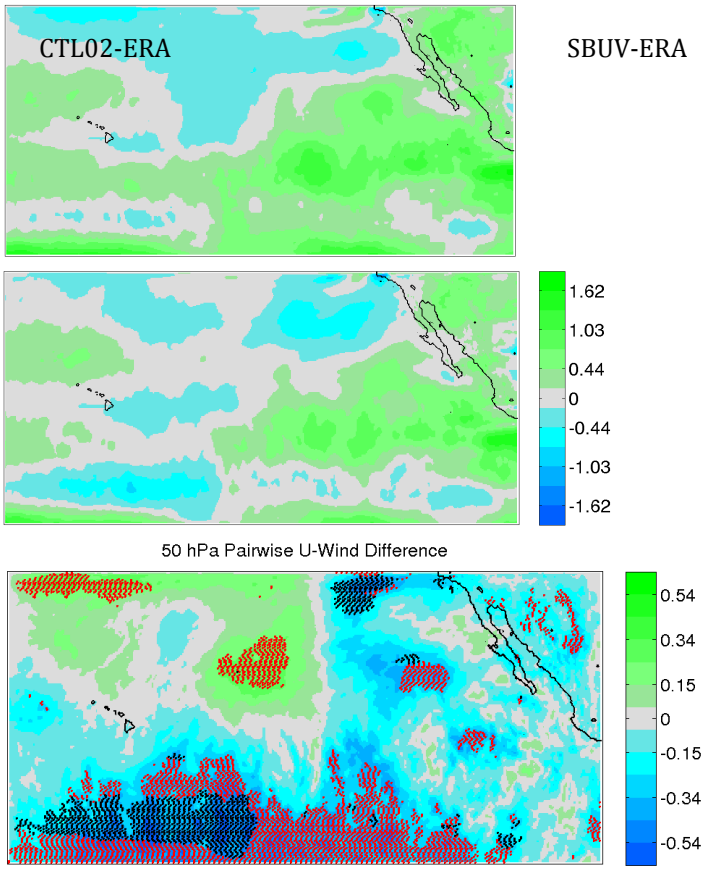

Figure 2.d-i.2.6: same as Figure 2.d-i.2.3 except 50 hPa zonal wind bias.

Figure 2.d-i.2.7 shows that although there are many SS differences for the specific humidity field, many of these SS differences are very small with a small difference reversing the sign on the SS difference comparison.

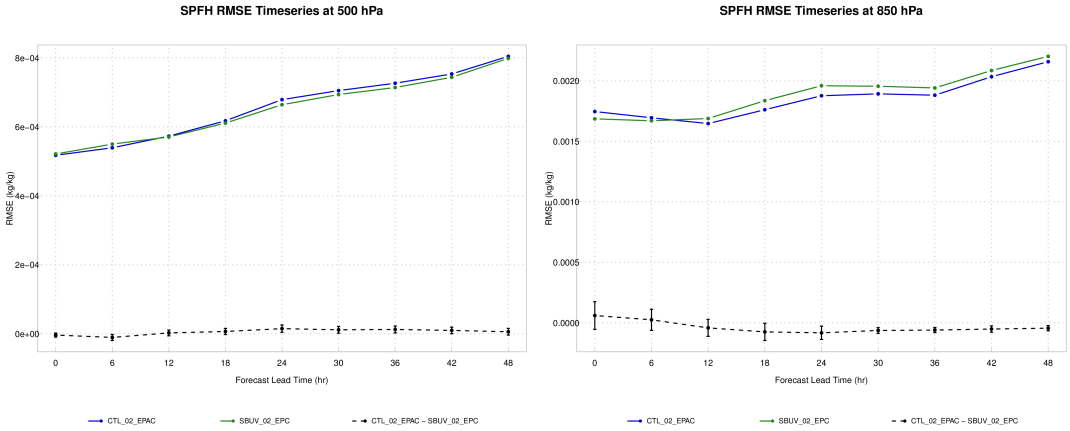

Figure 2.d-i.2.7: same as Figure 2.d-i.2.5 except specific humidity at 500 hPa (left) and 850 (hPa).

ii. GOME

GOME total ozone was assimilated into GSI with the same method as SBUV as a second source of ozone data to use in GSI with ARW for regional applications. GOME is a total

ozone product, which differs slightly from the SBUV profile ozone. Because the GOME sensor only records one time per day, the 12 UTC initializations only were aggregated for verification to isolate the impact of the GOME data.

Verification against the ERA-I reanalysis showed similar results to the SBUV comparison, but with fewer SS improvements (or degradations) and smaller magnitude differences. Table 2.d-ii.2.1 shows the SS table for bias, where the results are mixing for various variables. The RMSE SS table (Table 2.d-ii.2.2) shows fewer SS differences overall, with a clearer signal of upper-level temperature and wind improvements and mid-level degradations in temperature and zonal wind.

Table 2.d-ii.2.1: same as Table 2.d-i.2.1 except comparison between GOME (green) assimilation and control configuration (blue; following Air Force operational configuration).

99% CI Statistical Significance Table (bias): GOME vs. CTL02

TEMP Bias	Forecast Lead Time (hr)								
Pressure Levels (hPa)	0	6	12	18	24	30	36	42	48
50	EXPT	EXPT	--	CTRL	--	--	--	CTRL	--
100	EXPT	--	EXPT	--	--	--	--	--	--
250	EXPT	EXPT	--	--	--	--	--	--	--
400	--	CTRL	CTRL	--	--	--	--	--	--
500	--	--	--	--	--	--	--	--	--
700	--	CTRL	CTRL	CTRL	--	--	--	--	--
850	CTRL	CTRL	CTRL	CTRL	CTRL	CTRL	CTRL	CTRL	CTRL
925	--	--	EXPT	EXPT	EXPT	EXPT	EXPT	EXPT	EXPT

U-Wind Bias	Forecast Lead Time (hr)								
Pressure Levels (hPa)	0	6	12	18	24	30	36	42	48
50	CTRL	EXPT	EXPT	EXPT	CTRL	--	CTRL	EXPT	EXPT
100	CTRL	--	--	--	CTRL	--	--	--	CTRL
250	CTRL	CTRL	--	--	--	CTRL	CTRL	CTRL	CTRL
400	--	--	--	--	--	CTRL	CTRL	EXPT	--
500	--	--	EXPT	EXPT	EXPT	EXPT	EXPT	EXPT	CTRL
700	--	--	CTRL	--	--	CTRL	--	--	CTRL
850	--	CTRL	--	--	EXPT	CTRL	CTRL	--	CTRL
925	CTRL	CTRL	--	--	--	EXPT	CTRL	EXPT	EXPT

V-Wind Bias	Forecast Lead Time (hr)								
Pressure Levels (hPa)	0	6	12	18	24	30	36	42	48
50	CTRL	EXPT	EXPT	--	EXPT	CTRL	--	--	--
100	EXPT	--	--	CTRL	--	CTRL	--	CTRL	--
250	--	--	--	--	CTRL	--	--	--	--
400	--	CTRL	CTRL	--	CTRL	CTRL	--	EXPT	EXPT
500	--	--	--	--	CTRL	EXPT	--	EXPT	EXPT
700	--	--	EXPT	EXPT	EXPT	EXPT	EXPT	CTRL	EXPT
850	CTRL	CTRL	--	CTRL	CTRL	--	--	EXPT	EXPT
925	CTRL	CTRL	CTRL	CTRL	CTRL	CTRL	CTRL	CTRL	--

SPFH Bias	Forecast Lead Time (hr)								
Pressure Levels (hPa)	0	6	12	18	24	30	36	42	48
50	--	--	--	--	--	--	--	--	--
100	--	--	--	--	--	--	--	--	--
250	--	CTRL	CTRL	CTRL	--	--	--	--	--
400	EXPT	CTRL	CTRL	CTRL	CTRL	CTRL	CTRL	CTRL	CTRL
500	--	--	CTRL	CTRL	CTRL	--	--	--	CTRL
700	EXPT	EXPT	EXPT	EXPT	EXPT	EXPT	EXPT	EXPT	EXPT
850	CTRL	CTRL	CTRL	CTRL	CTRL	CTRL	CTRL	CTRL	CTRL
925	EXPT	EXPT	EXPT	--	--	CTRL	CTRL	CTRL	CTRL

Table 2.d-ii.2.2: Same as Table 2.d-ii.2.1 except RMSE statistics.

99% CI Statistical Significance Table (RMSE): GOME vs. CTL02 (ATL)

TEMP RMSE	Forecast Lead Time (hr)								
Pressure Levels (hPa)	0	6	12	18	24	30	36	42	48
50	EXPT	EXPT	--	--	--	--	--	--	--
100	EXPT	--	--	--	--	--	--	--	EXPT
250	--	--	--	--	--	--	--	--	--
400	--	EXPT	--	--	--	--	--	--	--
500	--	EXPT	--	--	--	--	--	--	--
700	--	--	CTRL	CTRL	CTRL	CTRL	--	--	--
850	CTRL	CTRL	CTRL	CTRL	CTRL	CTRL	CTRL	CTRL	CTRL
925	EXPT	--	EXPT	EXPT	EXPT	EXPT	EXPT	EXPT	EXPT

U-Wind RMSE	Forecast Lead Time (hr)								
Pressure Levels (hPa)	0	6	12	18	24	30	36	42	48
50	EXPT	EXPT	--	EXPT	--	--	--	--	--
100	--	--	--	--	CTRL	--	EXPT	--	--
250	--	--	--	CTRL	CTRL	CTRL	CTRL	CTRL	CTRL
400	--	--	--	--	--	--	--	--	--
500	--	--	CTRL	--	--	--	--	--	--
700	--	--	--	--	--	--	--	--	--
850	--	EXPT	--	CTRL	CTRL	CTRL	CTRL	CTRL	CTRL
925	--	--	CTRL	CTRL	CTRL	CTRL	CTRL	--	--

V-Wind RMSE	Forecast Lead Time (hr)								
Pressure Levels (hPa)	0	6	12	18	24	30	36	42	48
50	EXPT	EXPT	EXPT	EXPT	EXPT	--	EXPT	EXPT	--
100	--	--	--	CTRL	--	--	--	--	--
250	--	--	--	--	--	--	--	--	--
400	EXPT	--	--	--	--	--	--	--	--
500	--	--	CTRL	--	CTRL	--	--	--	--
700	--	--	--	--	--	--	--	--	--
850	--	--	--	--	--	--	--	--	--
925	--	CTRL	--	CTRL	CTRL	CTRL	--	--	--

SPFH RMSE	Forecast Lead Time (hr)								
Pressure Levels (hPa)	0	6	12	18	24	30	36	42	48
50	--	--	--	--	--	--	--	--	--
100	--	--	--	--	--	--	--	--	--
250	CTRL	CTRL	--	--	--	--	--	--	--
400	CTRL	CTRL	CTRL	CTRL	CTRL	CTRL	CTRL	CTRL	CTRL
500	CTRL	CTRL	CTRL	CTRL	CTRL	CTRL	CTRL	CTRL	CTRL
700	EXPT	EXPT	EXPT	--	--	--	--	--	--
850	EXPT	--	--	--	CTRL	CTRL	CTRL	CTRL	CTRL
925	EXPT	--	--	EXPT	EXPT	EXPT	EXPT	EXPT	EXPT

Vertical temperature RMSE plots show similar trends to the SBUV comparison, but with fewer SS improvements with smaller magnitude differences in the earliest lead times, with SS differences fading earlier (by the 12-hour forecast time).

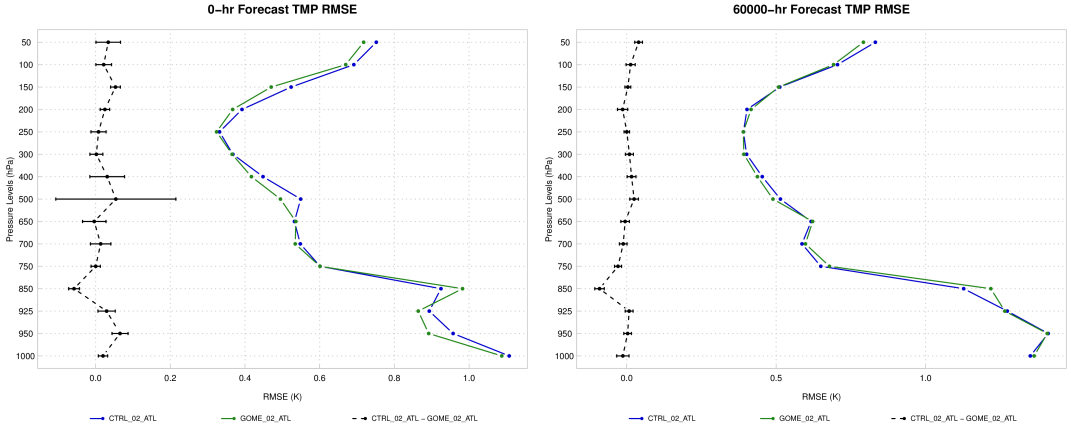

Figure 2.d-ii.2.1: same as 2.d-i.2.1 except comparison against GOME (green) and control configuration (blue).

Time series plots (Figure 2.d-ii.2.2) for 50 hPa and 500 hPa temperature once again show the early lead time improvement from the GOME assimilation, with differences quickly dissolving after 12 hours.

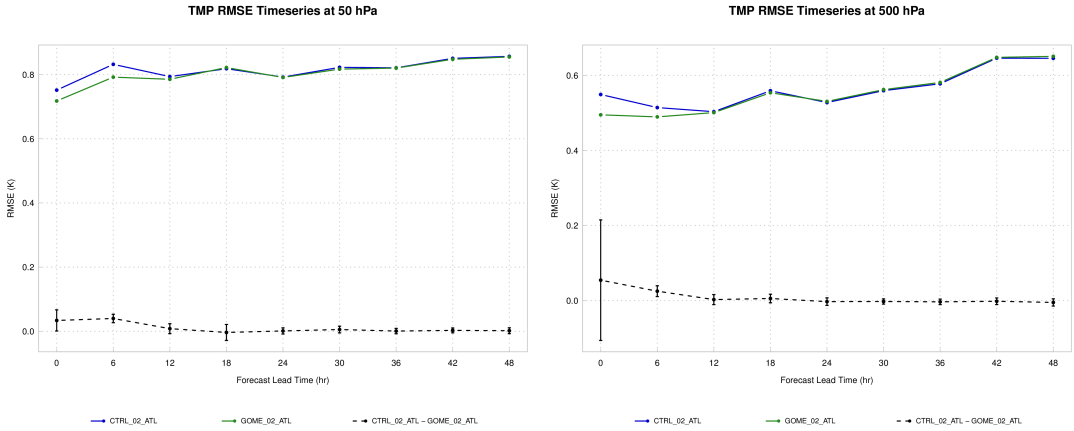

Figure 2.d-ii.2.2: same as 2.d-i.2.2 except GOME comparison (green) against control (blue) for 50 hPa and 500 hPa temperature RMSE.

Temperature biases at 150 hPa show the GOME configuration more similar to the ERA-I, with warmer temperatures in the control configuration in the northeast portion of the domain and temperatures cooler relative to ERA-I in the Caribbean. Differences over the mid-Atlantic are SS with differences favoring the GOME configuration, however there is a pocket of spatially coherent differences favoring the control configuration where the GOME configuration extended the cooler air too far into the Atlantic.

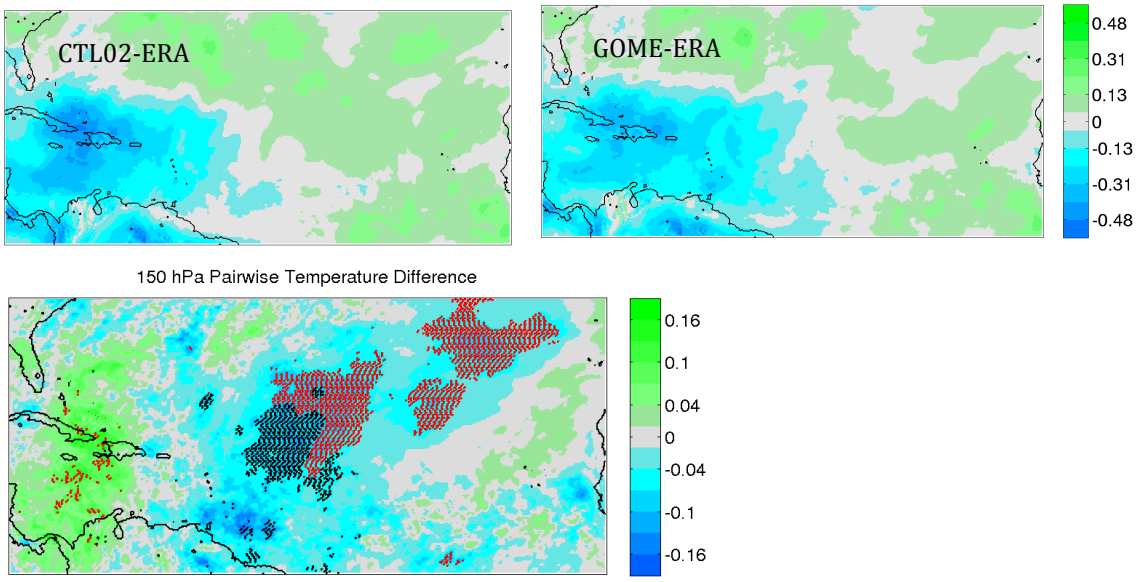

Figure 2.d-ii.2.3: same as 2.d-i.2.6, except 150 hPa temperature bias between GOME and the control configuration relative to ERA-I.

The GFS ozone was read in and interpolated to the regional grid to use as the background the GSI ozone assimilation. This is not done in the Air Force operational configuration;

therefore in addition to assimilating the ozone data, the GFS ozone background also provides a difference from the control configuration. Tables 2.d-ii.2.3 and 2.d-ii.2.4 show the SS pairwise differences when the control uses GFS ozone background (but does not assimilate any ozone data types). The results show a very similar result to those in Tables 2.d-ii.2.1 and 2.d-ii.2.2, indicating that adding the GFS ozone as the background does not change the control configuration dramatically, and the assimilation of the ozone data types is providing added benefit over the GFS ozone for the O-B.

Table 2.d-ii.2.3: same as 2.d-ii.2.1 except GFS ozone used in background for control.

99% CI Statistical Significance Table (bias): GOME vs. GFSOZ

TEMP Bias		Forecast Lead Time (hr)								
		0	6	12	18	24	30	36	42	48
Pressure Levels (hPa)	50	EXPT	EXPT	CTRL	CTRL	--	--	--	CTRL	--
	100	EXPT	CTRL	--	--	CTRL	--	--	--	--
	250	EXPT	EXPT	--	--	--	--	--	--	--
	400	--	--	--	--	--	--	--	--	--
	500	--	EXPT	EXPT	EXPT	EXPT	EXPT	EXPT	EXPT	--
	700	--	--	CTRL	CTRL	--	--	--	--	--
	850	CTRL	CTRL	CTRL	CTRL	CTRL	CTRL	CTRL	CTRL	--
	925	EXPT	EXPT	EXPT	EXPT	EXPT	EXPT	EXPT	EXPT	EXPT

U-Wind Bias		Forecast Lead Time (hr)								
		0	6	12	18	24	30	36	42	48
Pressure Levels (hPa)	50	CTRL	EXPT	--	EXPT	CTRL	--	--	EXPT	--
	100	--	--	CTRL	--	CTRL	EXPT	--	--	CTRL
	250	EXPT	CTRL	--	CTRL	EXPT	--	--	--	--
	400	CTRL	--	CTRL	CTRL	CTRL	--	CTRL	EXPT	--
	500	CTRL	--	EXPT	--	--	--	EXPT	EXPT	CTRL
	700	EXPT	--	--	CTRL	CTRL	--	--	--	CTRL
	850	--	CTRL	--	CTRL	CTRL	CTRL	CTRL	--	--
	925	CTRL	--	--	CTRL	CTRL	--	CTRL	EXPT	EXPT

V-Wind Bias		Forecast Lead Time (hr)								
		0	6	12	18	24	30	36	42	48
Pressure Levels (hPa)	50	--	--	EXPT	EXPT	EXPT	--	--	--	--
	100	--	--	--	CTRL	--	CTRL	CTRL	CTRL	--
	250	EXPT	CTRL	CTRL	--	CTRL	--	--	--	--
	400	--	CTRL	CTRL	--	CTRL	CTRL	--	EXPT	EXPT
	500	--	--	--	--	--	EXPT	CTRL	--	EXPT
	700	CTRL	--	EXPT	EXPT	--	--	EXPT	CTRL	EXPT
	850	CTRL	CTRL	EXPT	--	CTRL	--	--	--	--
	925	CTRL	CTRL	--	CTRL	CTRL	CTRL	CTRL	CTRL	--

SPFH Bias		Forecast Lead Time (hr)								
		0	6	12	18	24	30	36	42	48
Pressure Levels (hPa)	50	--	--	--	--	--	--	--	--	--
	100	--	--	--	--	--	--	--	--	--
	250	--	--	--	--	--	--	--	--	--
	400	CTRL	CTRL	CTRL	CTRL	CTRL	CTRL	CTRL	CTRL	CTRL
	500	--	--	--	--	--	--	--	--	--
	700	EXPT	EXPT	EXPT	EXPT	EXPT	EXPT	EXPT	EXPT	EXPT
	850	--	--	CTRL	CTRL	CTRL	CTRL	CTRL	CTRL	CTRL
	925	EXPT	EXPT	EXPT	--	CTRL	CTRL	CTRL	CTRL	CTRL

Table 2.d-ii.2.4: same as 2.d-ii.2.3 except RMSE statistics.

99% CI Statistical Significance Table (RMSE): GOME vs. GFSOZ

TEMP RMSE		Forecast Lead Time (hr)								
		0	6	12	18	24	30	36	42	48
Pressure Levels (hPa)	50	EXPT	EXPT	--	--	--	--	--	--	--
	100	EXPT	--	--	--	--	CTRL	CTRL	CTRL	--
	250	--	--	--	--	--	--	--	--	--
	400	--	--	--	--	--	--	--	--	--
	500	--	EXPT	--	EXPT	--	--	--	--	--
	700	CTRL	--	CTRL	CTRL	--	--	--	--	--
	850	CTRL	CTRL	CTRL	CTRL	CTRL	CTRL	CTRL	--	--
	925	--	--	--	EXPT	EXPT	EXPT	EXPT	EXPT	--

U-Wind RMSE		Forecast Lead Time (hr)								
		0	6	12	18	24	30	36	42	48
Pressure Levels (hPa)	50	EXPT	EXPT	--	EXPT	--	--	--	--	--
	100	--	--	--	--	CTRL	CTRL	--	--	--
	250	CTRL	CTRL	--	CTRL	--	--	--	--	--
	400	--	--	CTRL	CTRL	--	--	CTRL	--	CTRL
	500	--	CTRL	CTRL	CTRL	CTRL	CTRL	CTRL	CTRL	CTRL
	700	--	CTRL	CTRL	--	--	CTRL	--	--	--
	850	EXPT	--	--	CTRL	CTRL	--	--	--	--
	925	--	CTRL	CTRL	CTRL	CTRL	CTRL	--	--	--

V-Wind RMSE		Forecast Lead Time (hr)								
		0	6	12	18	24	30	36	42	48
Pressure Levels (hPa)	50	EXPT	--	EXPT	--	EXPT	--	EXPT	--	--
	100	--	--	--	CTRL	--	--	CTRL	--	--
	250	CTRL	CTRL	CTRL	CTRL	CTRL	--	--	--	--
	400	--	--	--	--	CTRL	--	--	--	--
	500	--	--	CTRL	--	--	--	--	--	--
	700	--	CTRL	--	--	--	--	--	--	--
	850	--	--	--	--	CTRL	--	--	--	--
	925	--	CTRL	--	--	CTRL	CTRL	--	--	--

SPFH RMSE		Forecast Lead Time (hr)								
		0	6	12	18	24	30	36	42	48
Pressure Levels (hPa)	50	--	--	--	--	--	--	--	--	--
	100	--	--	--	--	--	--	--	--	--
	250	--	--	--	--	--	--	--	--	--
	400	CTRL	CTRL	CTRL	CTRL	CTRL	CTRL	CTRL	CTRL	--
	500	CTRL	CTRL	CTRL	CTRL	CTRL	CTRL	CTRL	CTRL	CTRL
	700	EXPT	EXPT	EXPT	EXPT	--	--	--	--	--
	850	EXPT	EXPT	--	--	CTRL	CTRL	CTRL	CTRL	CTRL
	925	EXPT	--	--	EXPT	EXPT	EXPT	EXPT	EXPT	EXPT

e. CrIS data impact

The CrIS is a high-spectral resolution infrared instrument, which has over 1000 spectral channels and provides detailed and accurate observations on atmospheric temperature and moistures. The CrIS data impact test removed the CrIS data from the control configuration (the Air Force is already assimilating CrIS data in their operational system). Due to the large amount of radiance data already assimilated, as well as the redundancy with the AIRS overpasses and coverage in the domain (AIRS is another IR sensor, similar to the CrIS), the differences between the run with and without CrIS data assimilated showed very few SS differences. Figures 2e-i.2.1 and 2.e-i.2.2 show analysis and 12 hour forecast temperature bias; where the only notable SS differences occur in above 250 hPa in the analysis time, with SS differences fade by the 12-hour forecast time. Figure 2.e-i.2.3 also shows SS differences at the longer lead times for the v-component wind field, however these differences are also very small.

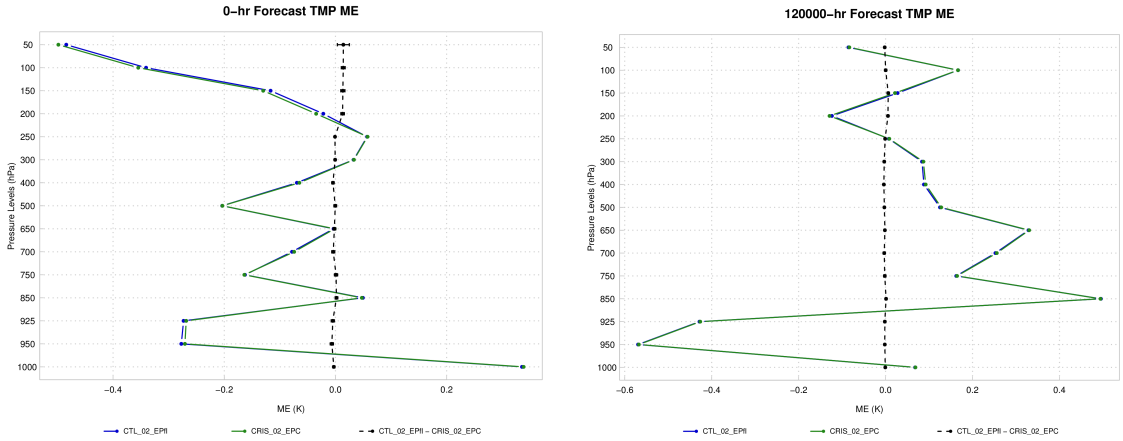

Figure 2.e-i.2.1: Vertical profile of mean temperature bias at the analysis (left) and the 12-hour forecast time (right) for the control configuration with CrIS (blue) and without CrIS data assimilated (green). The dashed black line indicates the pairwise differences. Differences are SS if the CI does not encompass zero.

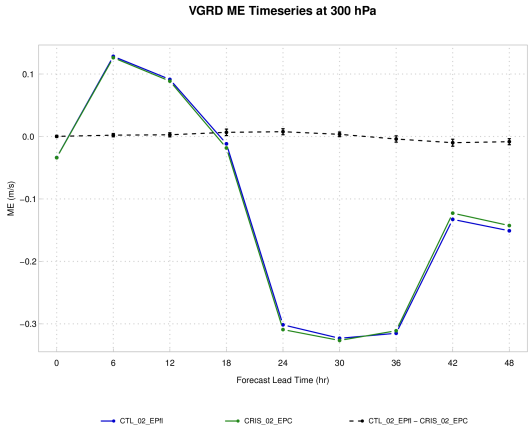

Figure 2.e-i.2.2: Timeseries for mean v-component wind bias at 300 hPa for the control configuration with CrIS (blue) and without CrIS assimilation (green). The dashed black line indicates the pairwise differences. Differences are SS if the CI does not encompass zero.

Although CrIS data have been shown to be a very good data source, the data overlap with the AIRS data may lessen the impact. Also, the channel selection for the CrIS configuration may need some careful consideration to improve the utility of these data based on a number of channels selected that are turned off in other regional operational configurations. Section f discusses the performance of the CrIS data in more detail with a focus on channel specific performance.

f. Sensitivity Tests Using GSI-based Forecast Sensitivity to Observations

Following the 2014 SOW (Statement of Work) for the DTC (Developmental Testbed Center) from the Air Force, observation sensitivity tests have been conducted using the GSI-based Forecast Sensitivity to Observations (FSO) Tools, adapted from the WRFDA-based FSO and developed by the Data Assimilation Team at NCAR/MMM. The system used in this work consists of version 3.6.1 of ARW (Advanced Research WRF) model, its tangent-linear and adjoint code (WRFPLUS, or WRF+) and the four-dimensional variational data assimlation (4DVAR) branch of the GSI code based on the community

GSI version 3.2 (Matching version of the FSO code was not available for the community GSI version 3.3). The implementation of this GSI-based FSO follows the diagram below (from Hui-Chuan Lin at NCAR/MMM, which was adapted from Liang Xu at NRL (Naval Research Laboratory)), which starts from the GSI 3DVAR analysis, followed by two nonlinear forecasts from the GSI analysis and background (the 6-hour forecast field from GFS analysis) respectively, forecast accuracy/error calculation using the GSI own analysis as the reference state, and the WRFPLUS to obtain the gradient of the forecast error with respect to the initial states, and the adjoint code of the GSI (GSI-4DVAR) to compute the impact of each observation on the forecast error reduction, using the Lanczos minimization.

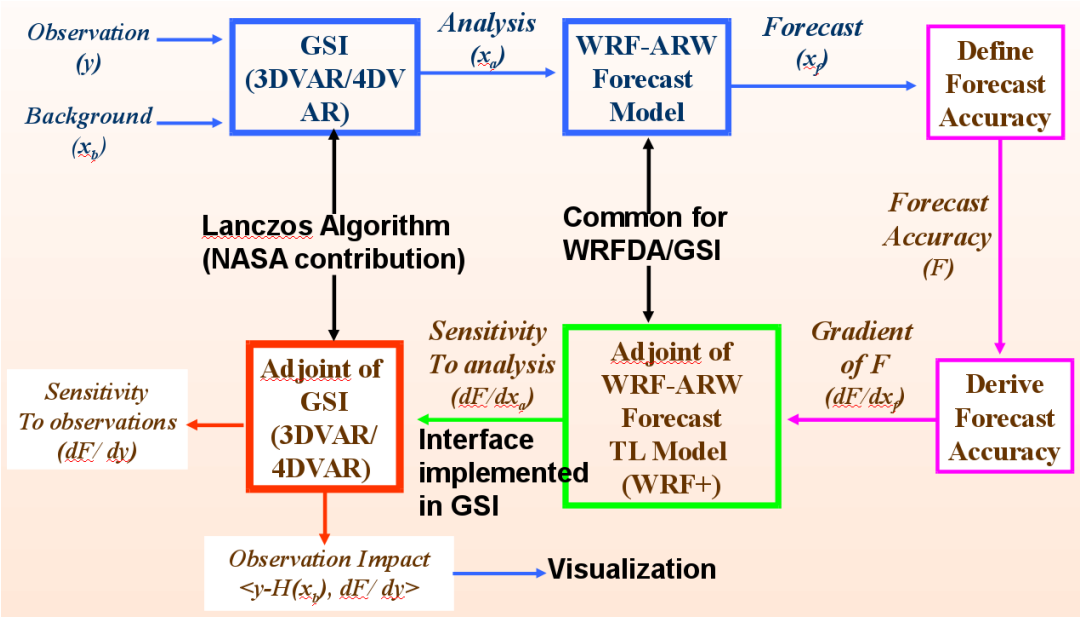

Figure 3.f-1: Schematic showing the implementation of the GSI-based FSO with ARW.

The domain for the FSO tests is the same as the one used in the data impact study for SBUV/2 (Solar Backscatter Ultraviolet Instrument) ozone data, extended from the eastern Pacific to the western continental US. The model resolution is 15km horizontally and it has 61 vertical levels, with the model top at 2mb. The testing period is 12 UTC 04 to 12 UTC 13, August 2014, with the focus on the impact on 12-hour forecasts. Besides the conventional observations and GPS (Global Positioning System) RO (Radio Occultation) data, the observation data includes

- SBUV/2 ozone profile from NOAA 19
- Satellite radiance data, including
  - AIRS (Atmospheric Infrared Sounder) from AQUA
  - AMSU (Advanced Microwave Sounding Unit)-A data from AQUA, NOAA 15, NOAA 18, NOAA 19
  - ATMS (Advanced Technology Microwave Sounder) from NPP (NPOESS Preparatory Project)
  - CrIS (Cross-track Infrared Sounder) from NPP
  - HIRS (High-resolution Infrared Radiation Sounder)-4 from NOAA 19
  - MHS (Microwave Humidity Sounder) from NOAA 18 and NOAA 19.

To facilitate the comparison with the data impact study, the radiance bias correction coefficients from the data impact study are used here. The GSI static files are the same as those used in the data impact study, including the background error covariance. Following the SOW, this work focuses on the impact of SBUV/2 ozone profile and CrIS from NPP, besides other radiance and conventional data.

The observation impact can be obtained from 1) the standard output from the GSI adjoint run, which gives an overall impact from each observation type and 2) the diag* files from the GSI adjoint run, which contain detailed information on the impact from each observation. Figure 3.f-2 gives the total averaged impact from ozone (oz) and radiance (rad) data (left) and the averaged impact per observation (right) on the 12-hour forecasts initialized at 00 UTC and 12 UTC. It shows forecast error reduction from ozone and radiance data, with radiance giving a large total impact and ozone giving a large impact per observation. Although the GSI codes used in this FSO study (based on community GSI v3.2) and the data impact study (community GSI v3.3) are different, this reduced forecast errors from SBUV/2 ozone data as seen in Figure 3.f-2 is consistent with what's been found in the data impact study, confirming the benefit of using the ozone profiles in the forecasts.

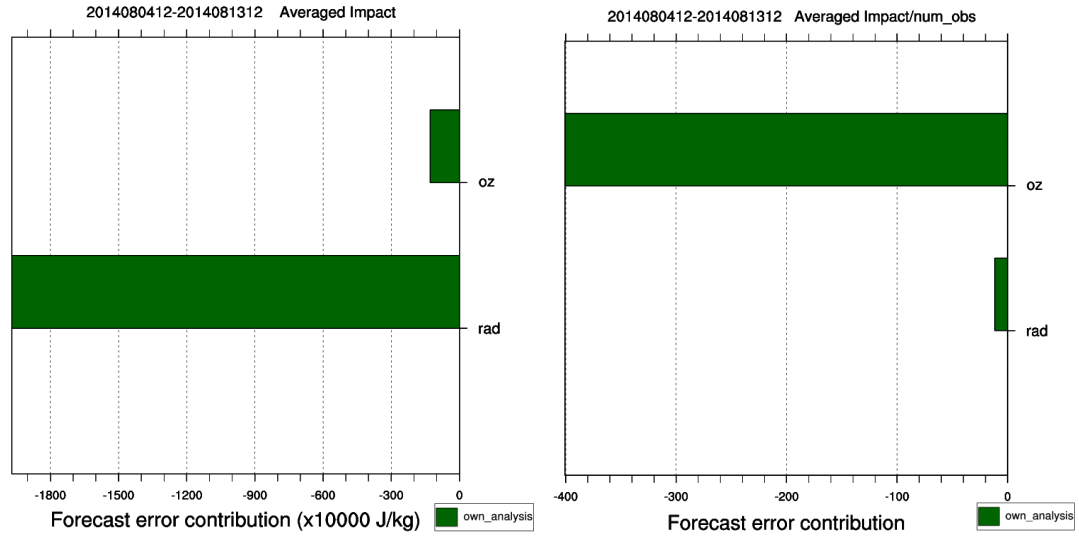

Figure 3.f-2: Overall impact from satellite radiance data (rad) and ozone profile (oz) on the 12-hour forecast initialized at 00 UTC and 12 UTC for the period of 04-13 August 2014.

Figure 3.f-3 gives the averaged impact from different satellite instruments for the 12-hour forecast initialized at 00 UTC and 12 UTC, showing reduced forecast errors from ATMS and AMSU-A, and increased forecast errors from MHS, HIRS4 and AIRS. Relatively large total impact is mainly from AMSU-A, especially AMUS-A from NOAA 18 and NOAA 15, while the largest impact per observation is from ATMS from NPP, followed by AMSU-A from NOAA 15 and NOAA 18.

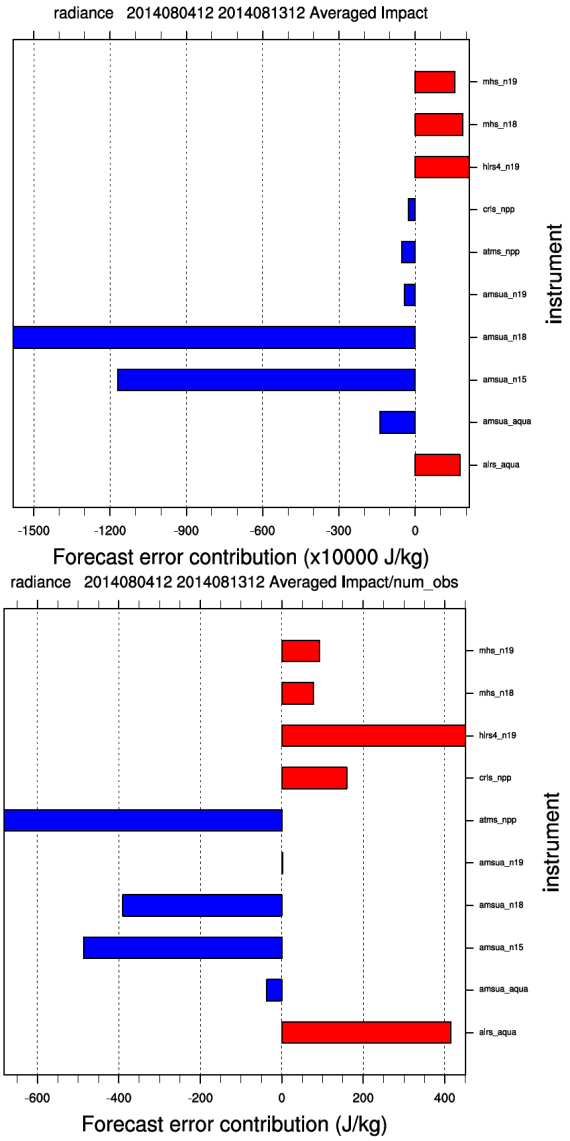

Figure 3.f-3: Observation impact from different satellite radiance instruments on the 12-hour forecast initialized at 00 UTC and 12 UTC for the period of 04-13 August 2014.

Note the total averaged impact from CrIS is slightly negative (suggesting reduced forecast errors) while the averaged impact per observation from CrIS is positive (suggesting increased forecast errors). However, considering the magnitude of the above contributions, the impact from CrIS is neutral, which is also consistent with the findings from the data impact study. Another look at the impact from CrIS is presented in figure 3.f-4, showing the forecast error contributions from individual channels at both 00 UTC and 12 UTC is very small (~ -3 * 10^4 J/kg for total contribution and ~ -25 to 40 J/kg for contribution per observation) compared to the one from AMSU-A from NOAA 18 (~ -1500 *10^4 J/kg for total contribution and ~ -400 J/kg for contribution per observation). The forecast error reduction from CrIS is mainly from channels 37-99, with largest impact from channel 53, 63 and 37. Channels 101-342 gives increased forecast errors and channels 392-713 gives small forecast error reduction. When breaking down the CrIS

impact into different initialization times (Figure 1.5), almost opposite impacts are found at 00 UTC and 12 UTC, with 00 UTC gives more forecast error reductions and 12 UTC gives more forecast error increases.

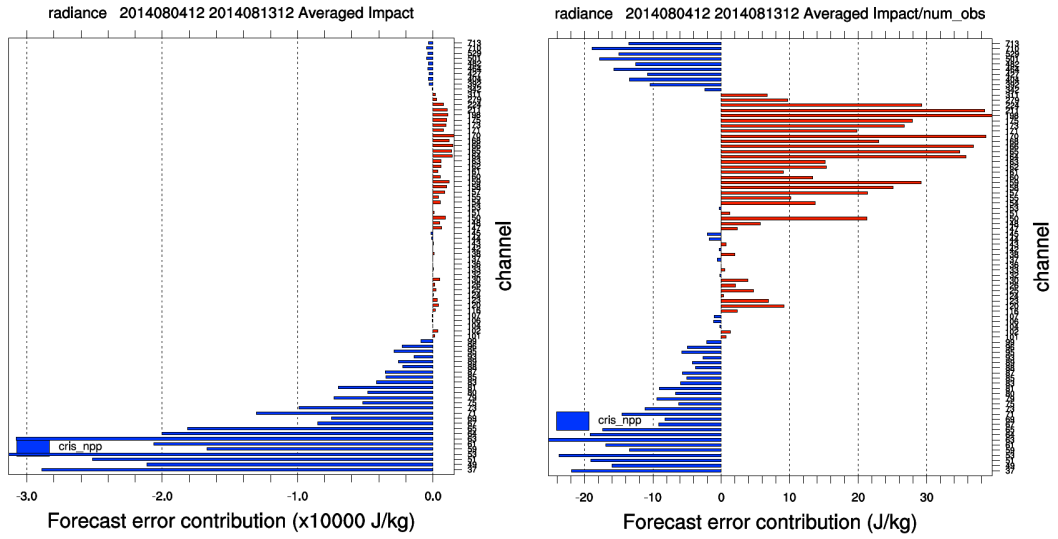

Figure 3.f-4: Observation impact from different CrIS channels on the 12-hour forecast initialized at both 00 UTC and 12 UTC for the period of 04-13 August 2014.

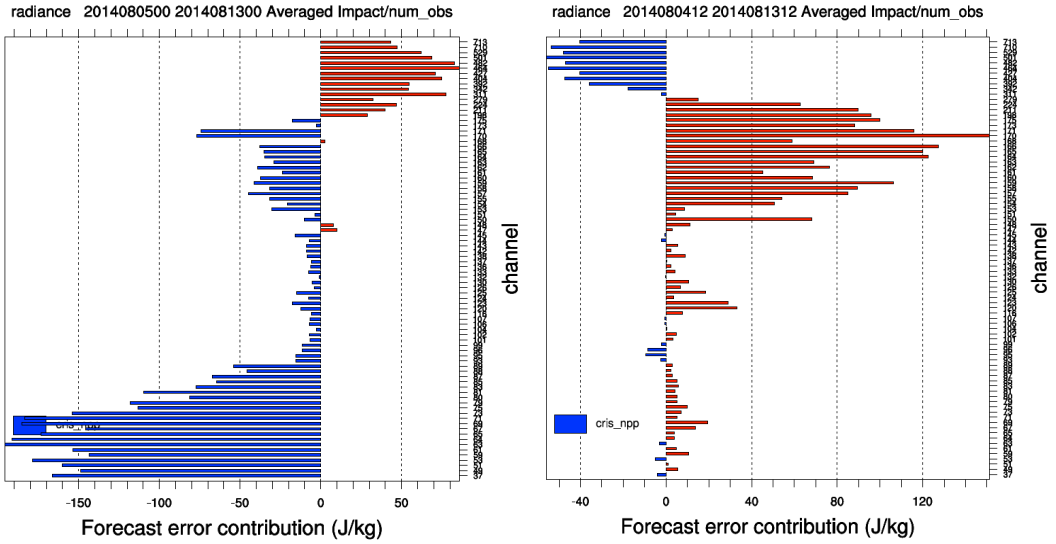

Figure 3.f-5: Observation impact per observation from different CrIS channels on the 12-hour forecast initialized at 00 UTC (left) and 12 UTC (right) for the period of 04-13 August 2014.

To provide more detailed recommendations on the satellite platform/channel selection, the channel specific impacts are also examined for other instruments. Figure 1.6 gives the averaged contribution from different channels of AIRS from AQUA, in which the total impact ranges from $-30*10^4$ to $20*10^4$ J/kg and the impact per observation ranges from -80 to 70 J/kg, and only a small fraction of the channels give reduced forecast errors. Table 1.1 summarizes the channel specific impact for AMUS-A and ATMS. For AMSU-A, channel 10 seems to contribute the most to the reduced forecast errors. For both

AMSU-A and ATMS, runs initialized at 00 UTC tend to be associated with more reduced forecast errors while runs initialized at12 UTC tend to be associated with more increased forecast errors.

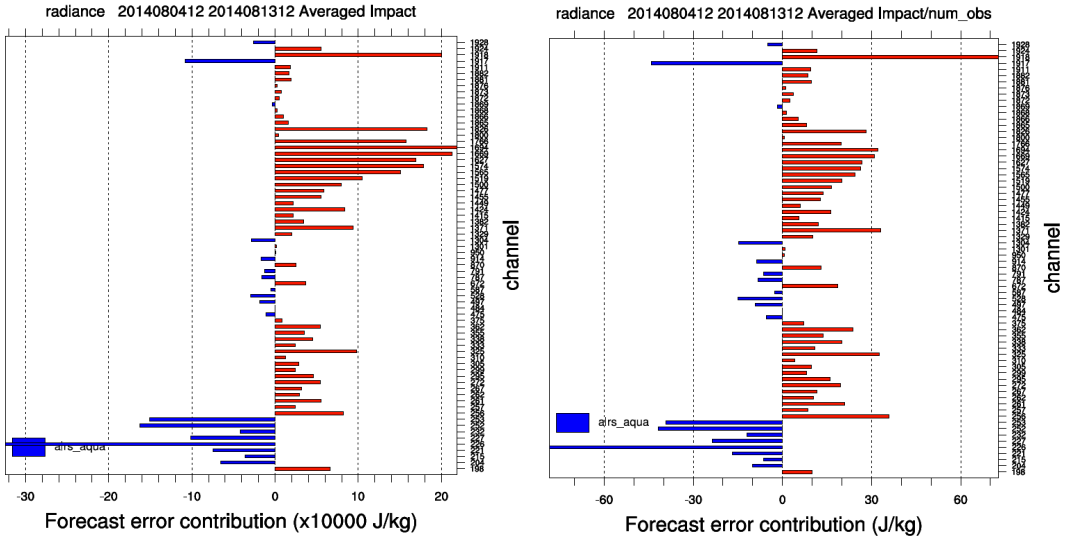

Figure 3.f-6: Observation impact from different AIRS channels on the 12-hour forecast initialized at both 00 UTC and 12 UTC for the period of 04-13 August 2014.

Table 3.f-1: Channel specific impact on the forecast errors for AMSU-A and ATMS, with channels with large error reduction in blue.

Satellite instruments		Channels with reduced forecast errors			Channels with increased forecast errors		
		Total (00Z and 12Z)	00Z	12Z	Total (00Z and 12Z)	00Z	12Z
AMSU-A	AQUA	10	6, 8, 9, **10**		6, 8, 9		6, 8, 9, 10
	NOAA 15	3, 6, 7, 8, 9, **10**	6, 7, 8, 9, **10**	3, 6, 7, 10	1, 2, 4, 5, 15	1-5,15	1, 2, 5, 8, 9, 15
	NOAA 18	5, 8, **10**	5, 7, **10**	8	1, 3, 4, 6, 15	1, 2, 4, 6, 15	1-7, 10, 15
	NOAA 19	9, **10**	9, **10**	15	1-7, 15	1-7, 15	1-7, 9, 10
ATMS	NPP	1-3, 9-14, 16-17	7-14, 16-20, 22	1, 2, 13, 14	4, 5-8, 20-22	5, 6	3-12, 20-22

g. Conclusions

The model top test showed convincingly that the 2 hPa model top configuration improved the statistics for the higher peaking AMSU-A channels, as well as consistent improvement in forecast skill for the entire forecast period. When focusing on the utility of ozone data in the GSI when coupled with ARW, there are signs of improvement, particularly in the earliest lead times upper-levels for temperature and wind. The SBUV assimilation showed a bit more promising with a slightly stronger signal for improvement and larger SS differences over the control configuration. Tests using the GFS ozone background in the control indicated that assimilating ozone data for use in the CRTM, and not propagating the variable into the forecast model does have value over simply

adding GFS ozone to the background. Finally, the CrIS impact test indicating that there was no added forecast benefit additionally over the current operational suite, which includes both AIRS and IASI. FSO tests indicate that careful channel selection may help improve the utility of the CrIS data. Additionally, the FSO analysis indicated forecast error reduction from the ozone and radiance data, supporting the data impact experiments.

4. Appendix

a. GSI namelist

```
&SETUP
   miter=2,niter(1)=100,niter(2)=70,
   write_diag(1)=.true.,write_diag(2)=.false.,write_diag(3)=.true.,
   gencode=78,qoption=2,
   factqmin=0.0,factqmax=0.0,deltim=1200,
   ndat=87,iguess=-1,
   oneobtest=.false.,retrieval=.false.,
   nhr_assimilation=3,l_foto=.false.,
   use_pbl=.false.,
   regional_ozone=.false.,
   use_gfs_ozone=.true.,
   check_gfs_ozone_date=.false.,
   use_gfs_stratosphere=.false.,
/
 &GRIDOPTS
   JCAP=62,JCAP_B=,NLAT=,NLON=,nsig=60,regional=.true.,
   wrf_nmm_regional=.false.,wrf_mass_regional=.true.,
   diagnostic_reg=.false.,
   filled_grid=.false.,half_grid=.true.,netcdf=.true.,
 /
 &BKGERR
   vs=1.0,
   hzscl=0.373,0.746,1.50,
   bw=0.,fstat=.true.,
 /
 &ANBKGERR
 /
 &JCOPTS
 /
 &STRONGOPTS
 /
 &OBSQC

dfact=0.75,dfact1=3.0,noiqc=.false.,c_varqc=0.02,use_poq7=.true.,qc_noi
rjaco3=.true.,vadfile='prepbufr',
 /
```

b. ARW namelist

```
&time_control
&dfi_control
&domains
 time_step                           = 60,
 time_step_fract_num                 = 0,
 time_step_fract_den                 = 1,
 max_dom                             = 1,
 max_dz                              = 1200
 s_we                                = 1,     1,     1,
 e_we                                = 481, 321, 157,
```

```
 s_sn                                = 1,     1,     1,
 e_sn                                = 241, 301, 154,
 s_vert                              = 1,     1,     1,
 e_vert                              = 62,    51,    51,
 num_metgrid_levels                  = 48,
 num_metgrid_soil_levels             = 4,
 dx                                  = 15000.0, 3000.0, 1000.0,
 dy                                  = 15000.0, 3000.0, 1000.0,
 grid_id                             = 1,     2,     3,
 parent_id                           = 0,     1,     2,
 i_parent_start                      = 0,  153,  166,
 j_parent_start                      = 0,  159,  141,
 parent_grid_ratio                   = 1,  4,3,
 parent_time_step_ratio              = 1,  3,3,
 feedback                            = 0,
 smooth_option                       = 0
 p_top_requested                     = 200
 interp_type                         = 2
 lowest_lev_from_sfc                 = .false.
 lagrange_order                      = 1
 force_sfc_in_vinterp                = 12
 zap_close_levels                    = 1
/

 &physics
 mp_physics                          = 4,     6,     6,
 ra_lw_physics                       = 4,     1,     1,
 ra_sw_physics                       = 4,     1,     1,
 radt                                = 30,    30,    30,
 o3input                             = 2,
 aer_opt                             = 1,
 sf_sfclay_physics                   = 1,     1,     1,
 sf_surface_physics                  = 2,     3,     3,
 bl_pbl_physics                      = 1,     1,     1,
 bldt                                = 0,     0,     0,
 cu_physics                          = 1,     1,     0,
 cudt                                = 5,
 isfflx                              = 1,
 ifsnow                              = 0,
 icloud                              = 1,
 surface_input_source                = 1,
 num_soil_layers                     = 4,
 mp_zero_out                         = 2,
 maxiens                             = 1,
 maxens                              = 3,
 maxens2                             = 3,
 maxens3                             = 16,
 ensdim                              = 144,
 num_land_cat                        = 24,
 fractional_seaice                   = 1,
 seaice_threshold                    = 0.0,
 tice2tsk_if2cold                    = .true.,
 /

 &fdda
 /

 &scm
```

```
 /

 &dynamics
 rk_ord                              = 3,
 diff_6th_opt                        = 2,
 diff_6th_factor                     = 0.10,
 w_damping                           = 1,
 diff_opt                            = 1,
 km_opt                              = 4,
 damp_opt                            = 3,
 base_temp                           = 290.,
 base_lapse_strat                    = -12.,
 iso_temp                            = 216.65,
 zdamp                               = 5000.,  5000.,  5000.,
 dampcoef                            = 0.05,    0.02,   0.01
 khdif                               = 0,      0,      0,
 kvdif                               = 0,      0,      0,
 SMDIV                               = 0.1,    0.1,    0.1,
 EMDIV                               = 0.01,   0.01,   0.01,
 EPSSM                               = 0.5,    0.1,    0.1
 non_hydrostatic                     = .true., .true., .true.,
 TIME_STEP_SOUND                     = 0,      4,      4,
 H_MOM_ADV_ORDER                     = 5,      5,      5,
 V_MOM_ADV_ORDER                     = 3,      3,      3,
 H_SCA_ADV_ORDER                     = 5,      5,      5,
V_SCA_ADV_ORDER                     = 3,      3,      3,
 moist_adv_opt                       = 1,      2,      2,
 scalar_adv_opt                      = 0,      2,      2,
 chem_adv_opt                        = 0,
 tke_adv_opt                         = 0,
 use_baseparam_fr_nml                = .true.,
 /
```